



UNIVERSITY OF LEEDS

This is a repository copy of *Carbon capture: Whole system experimental and theoretical modeling investigation of the optimal CO₂ stream composition in the carbon capture and sequestration chain*.

White Rose Research Online URL for this paper:
<http://eprints.whiterose.ac.uk/137751/>

Version: Accepted Version

Book Section:

Mahgerefteh, H, Porter, RTJ, Brown, S et al. (32 more authors) (2017) Carbon capture: Whole system experimental and theoretical modeling investigation of the optimal CO₂ stream composition in the carbon capture and sequestration chain. In: Mujtaba, IM, Srinivasan, R and Elbashir, NO, (eds.) *The Water-Food-Energy Nexus: Processes, Technologies, and Challenges*. Green Chemistry and Chemical Engineering . Taylor & Francis , pp. 553-602. ISBN 9781498760843

<https://doi.org/10.4324/9781315153209>

© 2018 by Taylor & Francis Group, LLC. This is an Accepted Manuscript of a book chapter published by Taylor & Francis in *The Water-Food-Energy Nexus* on 7/09/2017, available online: <https://doi.org/10.4324/9781315153209>.

Reuse

Items deposited in White Rose Research Online are protected by copyright, with all rights reserved unless indicated otherwise. They may be downloaded and/or printed for private study, or other acts as permitted by national copyright laws. The publisher or other rights holders may allow further reproduction and re-use of the full text version. This is indicated by the licence information on the White Rose Research Online record for the item.

Takedown

If you consider content in White Rose Research Online to be in breach of UK law, please notify us by emailing eprints@whiterose.ac.uk including the URL of the record and the reason for the withdrawal request.



eprints@whiterose.ac.uk
<https://eprints.whiterose.ac.uk/>

Whole System Experimental and Theoretical Modelling Investigation of the Optimal CO₂ Stream Composition in the Carbon Capture and Sequestration Chain

H. Mahgerefteh^{*a}, R.T.J. Porter^a, S. Brown^{a†}, S. Martynov^a, M. Fairweather^b, S.A.E.G. Falle^c, R.M. Woolley^b, G. Boulougouris^d, I. Economou^d, D.M. Tsangaris^d, A. Beigzadeh^e, C. Salvador^e, K.E. Zanganeh^e, A. Ceroni^f, R. Farret^f, Y. Flauw^f, J. Hébrard^f, D. Jamois^f, C. Proust^f, S.Y. Chen^g, J.L. Yu^g, Y. Zhang^g, D. Van Hoecke^h, R. Hojjati Talemi^h, S. Cooreman^h, J. Bensabatⁱ, R. Segevⁱ, D. Rebscher^j, J.L. Wolf^j, A. Niemi^k, C. Kolster^l, N. Mac Dowell^l, N. Shah^l

^aDepartment of Chemical Engineering, University College London, London WC1E 7JE, UK

^bSchool of Chemical and Process Engineering, University of Leeds, Leeds LS2 9JT, UK,

^cSchool of Mathematics, University of Leeds, Leeds LS2 9JT, UK

^dNational Center for Scientific Research “Demokritos”, Institute of Nanoscience and Nanotechnology, Molecular Thermodynamics and Modelling of Materials Laboratory, Aghia Paraskevi, Attikis GR–153 10, Greece

^eCanmetENERGY, Natural Resources Canada, Ottawa, K1A 1M1, Canada

^fINERIS, Parc Technologique ALATA, Verneuil-en-Halatte BP 2, 60550, France

^gSchool of Chemical Engineering, Dalian University of Technology, Dalian, People's Republic of China

^hArcelorMittal Global R&D Gent-OCAS NV, Pres. J.F. Kennedylaan 3, 9060 Zelzate, Belgium^hUniversity of Leeds, UK

ⁱEnvironmental and Water Resources Engineering Ltd, Haifa, Israel

^jBundesanstalt für Geowissenschaften und Rohstoffe (BGR), Geozentrum Hannover, Stilleweg 2, 30655 Hannover, Germany

^kUppsala University, Department of Earth Sciences, Villavägen 16, SE-75236 Uppsala, Sweden

^lCentre for Process Systems Engineering, Department of Chemical Engineering, Imperial College London, London SW7 2AZ, UK

[†]Current address: Department of Chemical and Biological Engineering, University of Sheffield, Sheffield, London S1 3JD, UK.

*Coordinator and corresponding author: h.mahgerefteh@ucl.ac.uk

40.1 Introduction

CO₂ Capture and Storage (CCS) refers to a collection of technologies which allow for the continued use of fossil fuels for energy generation and heavy industries while abating their atmospheric emissions of the greenhouse gas carbon dioxide (CO₂) by capturing it in the given process, and then transporting it to a suitable location for subsurface geological storage. For large-scale applications of CCS, transport of CO₂ using pressurised pipelines is found to be the most practical and economic method [1]. However, the CO₂ stream captured from fossil fuel power plants or other CO₂ intensive industries will contain a range of different types of impurities each having its own impact on the different parts of the CCS chain.

Determining the ‘optimum composition’ of the captured CO₂ stream addressing the cost, safety and environmental concerns is therefore fundamentally important in facilitating CCS as a viable technology for addressing the impact of global warming.

This Chapter presents the main issues and provides an overview of the experimental and theoretical modelling work carried out as part of the CO₂QUEST European Commission Collaborative Project [2] tasked with addressing this challenge.

40.1.1 Classes of CO₂ Impurities by Origin

Impurities contained in the CO₂ streams from different carbon capture technologies may be classified broadly by origin into three main categories arising from fuel oxidation, excess oxidant/air ingress, and process fluids as shown in Table 1 [3]. Water is a major combustion product and is considered an impurity in the CO₂ stream. The elements inherently present in a fuel such as coal include sulphur, chlorine and mercury, and are released upon complete or incomplete combustion and form compounds in the gas phase which may remain to some extent as impurities in the CO₂ after it is captured and compressed. The oxidising agent used for combustion such as air may result in residual impurities of N₂, O₂ and Ar; these same impurities may also result from any air ingress into the process. The materials and chemicals used for the CO₂ separation process such as monoethanolamine (MEA) used for post-

combustion capture or Selexol in pre-combustion capture and their degradation products can be carried over into the CO₂ stream constituting a further class of impurity.

Table 1. Classes of potential CO₂ impurities by origin.

| Coal/biomass oxidation products | |
|--|--|
| Complete | Partial |
| H ₂ O, SO _x , NO _x , HCl, HF | CO, H ₂ S, COS, NH ₃ , HCN |
| Volatiles | Biomass alkali metals |
| H ₂ , CH ₄ , C ₂ H ₆ , C ₃ ⁺ | KCl, NaCl, K ₂ SO ₄ , KOH etc. |
| Trace metals | Particulates |
| Hg (HgCl ₂), Pb, Se, As etc. | Ash, PAH/soot |
| Oxidant / air ingress | Process fluids |
| O ₂ , N ₂ , Ar | Glycol, MEA, Selexol, NH ₃ etc. |

40.1.2 Impacts of CO₂ impurities on CCS systems

Impurities that arise from CO₂ capture sources can have a number of important impacts on the downstream transport and storage infrastructure and operation. The presence of impurities in CO₂ the total concentration, such as the air derived non-condensable species (N₂, O₂ and Ar), can shift the boundaries in the CO₂ phase diagram to higher pressures, meaning that higher operating pressures are needed to keep CO₂ in the dense phase and hence impacting on compression and transport costs. In addition, these species can reduce the CO₂ structural trapping capacity in geological formations by a greater degree than their molar fractions [4] Hydrogen may be present in pre-combustion capture derived CO₂ streams and is also believed to impact required pipeline inlet pressures significantly [5]. Enhanced Oil Recovery (EOR) applications require stricter limits, particularly on O₂ due to it promoting microbial growth and reaction with hydrocarbons. Water should be limited in CCS applications in order to mitigate corrosion due to the formation of in situ carbonic acid [6], clathrate formation and condensation at given operating conditions [1]. On the other hand, water may be of benefit even at high concentrations in storage given its immobilisation effect on CO₂.

Sulfur species (H₂S, COS, SO₂ and SO₃) may pose a corrosion risk in the presence of water and there are additional toxicity concerns for H₂S. NO_x species may be present in CO₂ streams as combustion by-products and also pose a corrosion risk due to nitric acid formation [7]. Trace elements such as Lead, Mercury and Arsenic in the CO₂ stream are of concern for geological storage due to their toxicity and the possibility that they could contaminate groundwater. Amongst the numerous potential trace metal CO₂ impurities, mercury receives further attention for its corrosive effects on a number of metals. Due to its toxicity, limits are also suggested for carbon monoxide. For other components that may be present in CO₂ streams (e.g., HCl, HF, NH₃, MEA, Selexol), not enough information is available to fully understand their downstream impacts on transport and storage and determine maximum allowable amounts. Further work is therefore required to understand the impacts of these species in transport and storage applications and to elucidate potential crossover effects.

40.1.3 The QUEST for “optimal” CO₂ purity

In CCS systems, as illustrated in Figure 1, capture costs can be expected to increase with CO₂ purity when additional process unit operations and increased energy penalty associated with achieving the desired CO₂ purity is taken into consideration. Conversely, transport and storage costs (per tonne of CO₂ transported), as depicted in Figure 1, may be expected to decrease with increasing CO₂ purity due to the lower compression requirements to keep CO₂ in the dense phase, lower rates of corrosion and the relaxation of safety measures needed to deal with hazardous impurities. When capital and operating costs are factored together to calculate a levelised “total cost” for CCS systems, a minima for a given purity and composition range is expected where the system may be assumed to be cost optimised in addition to having the necessary safety precautions taken into consideration. The challenge therefore is to find optimum range and concentration of impurities that can be permitted in the CO₂ stream to enable its safe and cost-effective transportation and storage.

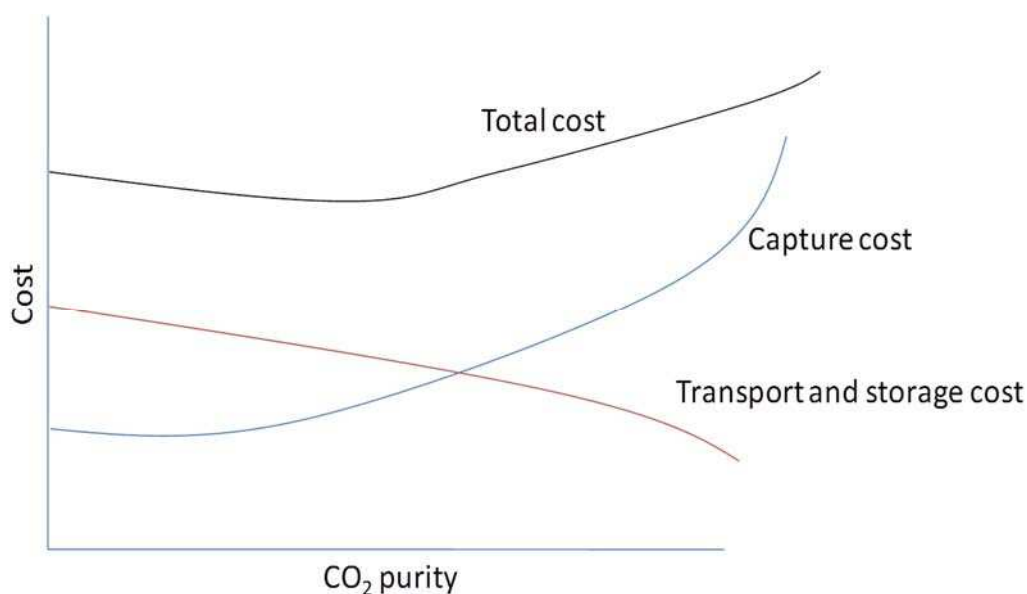


Figure 1. Cost trade-offs associated with CO₂ purity.

The CO₂QUEST project [2] addresses the fundamentally important issues surrounding the impact of the typical impurities in the CO₂ stream captured from fossil fuel power plants and other CO₂ intensive industrial emitters on its safe and economic pipeline transportation and storage. This 40 months duration project funded by the European Commission under the FP7 framework programme commenced in February 2013. It involves the collaboration of 10 academic and industry partners across Europe, China and Canada.

This chapter presents an overview of the project and some of its main findings. Key gaps in knowledge relating to the impact of impurities on the chemical, physical and transport properties of the captured CO₂ stream under different operating conditions are addressed.

40.2 Project Work Packages

Figure 2 shows a schematic representation of the CO₂QUEST work programme divided into 7 Work Packages (WP), encompassing technical (WP1 to WP5), dissemination (WP6) and project management (WP7) activities. The following is a description of each of the technical WP's, their interactions with other WP's and the main findings.

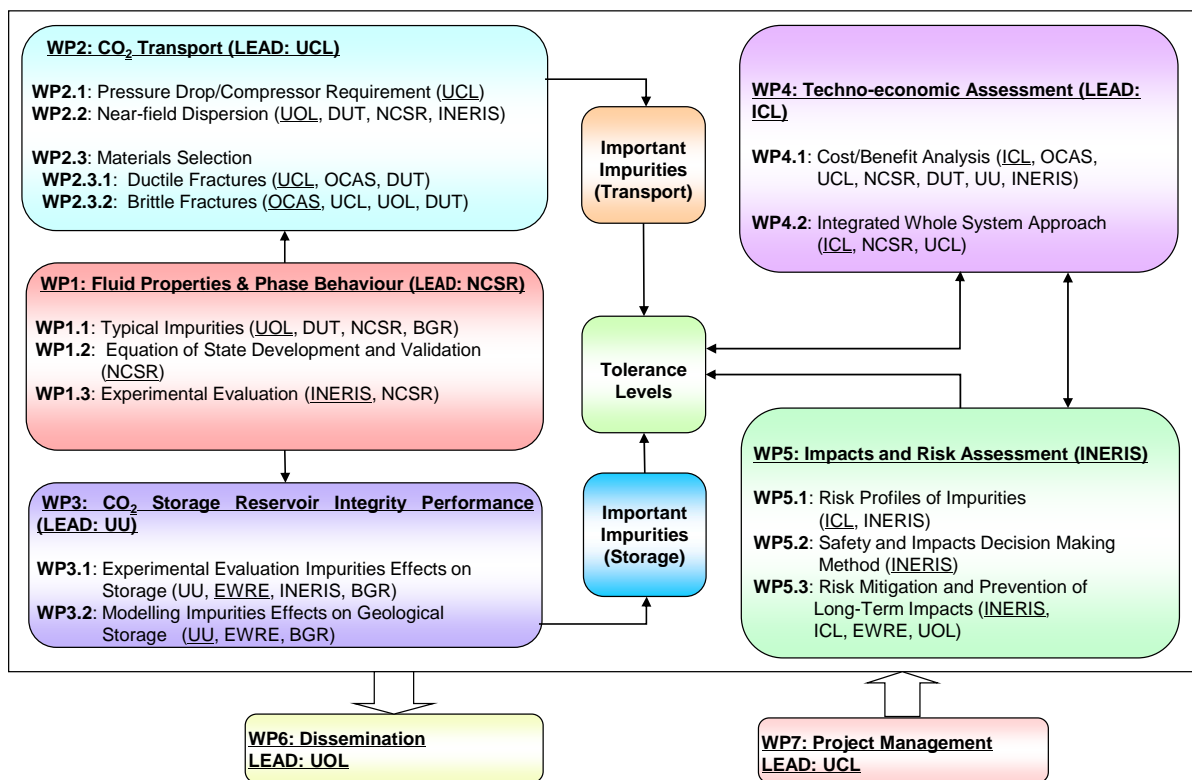


Figure 2. CO₂QUEST work programme structure.

40.2.1 WP1 – Fluid properties and phase behaviour

40.2.1.1 WP1.1 – Typical impurities and cost-benefit analysis

The work in this section underpins the other project activities by providing analysis of the ranges and levels of impurities present in CO₂ streams derived from different carbon capture sources, including those from both the power sector and heavy industries based on literature studies. The factors that affect the ranges and levels of impurities for given power generation technologies, such as post-combustion, pre-combustion and oxyfuel combustion capture, have also been identified leading to the ranges as set out in Table 2.

Table 2. CO₂ impurities from different CO₂ capture technologies.

| | Oxyfuel Combustion | | | Pre-combustion | Post-combustion |
|--------------------------------|--------------------|-----------------|--------------|----------------|-----------------|
| | Raw / dehumidified | Double flashing | Distillation | | |
| CO₂ % v/v | 74.8-85.0 | 95.84-96.7 | 99.3-99.9 | 95-99 | 99.6 – 99.8 |
| O₂ % v/v | 3.21-6.0 | 1.05-1.2 | 0.0003-0.4 | 0 | 0.015 – 0.0035 |
| N₂ % v/v | 5.80-16.6 | 1.6-2.03 | 0.01-0.2 | 0.0195 – 1 | 0.045 - 0.29 |
| Ar % v/v | 2.3-4.47 | 0.4-0.61 | 0.01-0.1 | 0.0001-0.15 | 0.0011 – 0.021 |
| NO_x ppmv | 100-709 | 0-150 | 3-100 | 400 | 20 - 38.8 |
| SO₂ ppmv | 50-800 | 0-4500 | 1-50 | 25 | 0 - 67.1 |
| SO₃ ppmv | 20 | - | 0.1-20 | - | N.I. |
| H₂O ppmv | 100-1000 | 0 | 0-100 | 0.1 - 600 | 100 – 640 |
| CO ppmv | 50 | - | 2-50 | 0 - 2000 | 1.2 - 10 |
| H₂S/COS ppmv | | | | 0.2 - 34000 | |
| H₂ ppmv | | | | 20-30000 | |
| CH₄ ppmv | | | | 0-112 | |

A techno-economic modelling study of power plants with CO₂ capture technologies with focus on process scenarios that deliver different grades of CO₂ product purity was also carried out in this work package. The three leading CO₂ capture technologies for the power sector are considered, namely; oxyfuel combustion, pre-combustion and post-combustion capture. The study uses a combination of process simulation of flue gas cleaning processes, modelling with a power plant cost and performance calculator and literature values of key performance criteria in order to calculate capital costs, operational and maintenance costs, the levelised cost of electricity and CO₂ product purity of the considered CO₂ capture options.

For oxyfuel combustion capture, the calculations are based on a 400 MWg retrofitted power station that uses a low sulfur coal and considers three raw CO₂ flue gas processing strategies of compression and dehydration only, double flash system purification and distillation purification. Analysis of pre-combustion capture options is based on new build integrated gasification combined cycle plants with one gas-turbine and a GE entrained-flow gasifier. Integrated physical solvent systems for capturing CO₂ and sulfur species were considered in three ways; co-capture of sulfur impurities with the CO₂ stream using SelexolTM solvent, and separate capture of CO₂ and sulfur impurities using SelexolTM and Rectisol[®] solvent systems

for separate capture of sulfur impurities and CO₂. Analysis of post-combustion capture plants was made with and without some conventional pollution control devices.

Of the different cases considered, pre-combustion capture with co-capture of impurities and CO₂ using Selexol™ offered the lowest cost with reasonably high purity of CO₂ at 97.64 mol%, but high estimated levels of H₂S (at 3974 ppm_v) in the captured stream. The most expensive system was pre-combustion capture using Rectisol® with separate capture of CO₂ and sulfur impurities, producing a dry 99.51 mol% pure CO₂ stream. The system with the lowest grade of CO₂ was oxyfuel combustion capture with compression and dehydration of the raw CO₂ stream only, which resulted in 77.69 mol% pure CO₂ and with the second lowest cost. The oxyfuel plant with distillation purification system and the post-combustion capture plant with conventional pollution control devices had the joint highest CO₂ purity (99.99 mol%), with the post-combustion capture system estimated to be the cheaper of the two. The calculations performed are of use in further analyses of whole chain CCS for the safe and economic capture, transport and storage of CO₂.

40.2.1.1 WP1.2 – Equation of State Development and Validation

An integrated CCS process requires the transportation of a CO₂-rich stream from the capture plant to a sequestration site. Process simulation and design requires accurate knowledge of the physical properties of the mixtures transported through the pipeline and advanced equations of state (EoS) can be a very useful tool for the prediction and correlation of these properties [8,9] Moreover, an important consideration for the design and operation of CCS facilities is the understanding of the phase equilibria of the CO₂ mixtures associated with the process. Studying the vapor – liquid equilibrium (VLE) of these mixtures has attracted much attention both in terms of experimental measurements and modeling, but relatively little work has been performed to understand dry ice formation when other gases are present in the CO₂ stream. CO₂ exhibits a relatively high Joule – Thomson expansion coefficient and during transportation, a sudden pipeline depressurization will lead in rapid cooling so that very low temperatures can be reached [10]. Consequently, solidification of CO₂ may take place and this can affect the safety of CCS facilities during equipment depressurization or other process upsets [11,12].

In this WP, three solid thermodynamic models were applied to model the solid-fluid equilibrium (SFE) of pure CO₂ and CO₂ mixtures with other compounds, typically found in CO₂ streams from industrial sources, namely N₂, H₂ and CH₄. These models are an empirical correlation fitted on experimental data at SFE conditions, a thermodynamic integration model and a solid EoS developed for pure CO₂. The solid models have to be combined with a fluid EoS. In this work, the Peng-Robinson (PR), Soave-Redlich-Kwong (SRK) and Perturbed Chain-Statistical Associating Fluid Theory (PC-SAFT) EoS were used. All three fluid EoS are used widely for liquids and gases.

40.2.1.1.1 Solid Models

Empirical Correlation Model

SFE of a mixture requires that the chemical potentials of the solid former in the two coexisting phases (S: solid phase, F: fluid phase) are equal at the same temperature and pressure.

$$\mu_i^S(T, P) = \mu_i^F(T, P, \mathbf{x}^F) \quad (1)$$

where μ_i^S is the chemical potential of the solid former i in the pure solid phase and μ_i^F is its chemical potential in the coexisting fluid phase of molar composition \mathbf{x}^F . If the ideal gas reference state is used to calculate the chemical potential for both phases, eq. (1) can be substituted by the equation of fugacities [13]:

$$\hat{f}_i^S(T, P) = \hat{f}_i^F(T, P, \mathbf{x}^F) \quad (2)$$

and subsequently to the expression:

$$P_{0i}^{\text{sat}}(T) \hat{\varphi}_{0i}^{\text{sat}}(T, P_{0i}^{\text{sat}}) \exp \left[\frac{v_{0i}^S}{RT} (P - P_{0i}^{\text{sat}}(T)) \right] = x_i^F \hat{\varphi}_i^F(T, P, \mathbf{x}^F) P \quad (3)$$

where $P_{0i}^{\text{sat}}(T)$ is the saturation pressure of the pure solid former at temperature T , $\hat{\varphi}_{0i}^{\text{sat}}(T, P_{0i}^{\text{sat}})$ is the fugacity coefficient of the pure solid former at temperature T and pressure P_{0i}^{sat} , $\hat{\varphi}_i^F(T, P, \mathbf{x}^F)$ is the fugacity coefficient of the solid former in the fluid mixture of molar composition \mathbf{x}^F , at temperature T and pressure P , and v_{0i}^S is the temperature and pressure independent pure solid molar volume.

Eq. (3) can be employed to calculate the SFE of a multicomponent mixture with the use of a fluid EoS for the fugacity coefficients and a model that provides the saturation pressure of the solid former at SLE or SVE conditions, which can be an empirical correlation fitted to experimental data.

Thermodynamic Integration Model

Seiler et al. [14] proposed a different methodology for SFE modeling. In their approach, for SLE calculation, the reference state is the pure, subcooled melt, at system temperature and standard pressure (P^+), while P^+ is selected accordingly by taking into account the existence of caloric data at this reference state. The expression that applies to the SLE with this model is:

$$x_i^L = \frac{\varphi_{0i}^{L*}}{\varphi_i^L} \cdot \exp \left[-\frac{(v_{0i}^S - v_{0i}^{L*})(P^+ - P)}{RT} - \frac{\Delta h_{0i}^{SL}}{RT} \left(1 - \frac{T}{T_{0i}^{SL}} \right) + \frac{\Delta c_{P,0i}^{SL*}}{RT} (T_{0i}^{SL} - T) - \frac{\Delta c_{P,0i}^{SL*}}{R} \ln \frac{T_{0i}^{SL}}{T} \right] \quad (4)$$

where Δh_{0i}^{SL} is the enthalpy of melting at melting temperature T_{0i}^{SL} , v_{0i}^S and v_{0i}^{L*} are the pure solid former solid molar volume and liquid molar volume at the solid-liquid transition and $\Delta c_{P,0i}^{SL*}$ is the difference of the molar, isobaric heat capacities between the hypothetical subcooled melt and the solid.

Gibbs Free Energy Equation of State for Solid CO₂

Jager and Span [15] developed an empirical EoS that describes the thermodynamic behavior of solid CO₂, which is explicit in the Gibbs free energy. A fundamental expression for the Gibbs free energy is used and is fitted to appropriate experimental data of solid CO₂. The Gibbs free energy can be fundamentally written as:

$$g(P, T) = h_0 - Ts_0 + \int_{T_0}^T c_P(T, P_0) dT - T \int_{T_0}^T \frac{c_P(T, P_0)}{T} dT + \int_{P_0}^P v(P, T) dP \quad (5)$$

By using appropriate functional forms for the heat capacity, the expansion coefficient and the partial derivative of the molar volume with respect to pressure, these quantities can be accurately fitted to experimental data. The resulting expression for the Gibbs free energy is:

$$\begin{aligned} \frac{g}{RT_0} = & g_0 + g_1 \Delta\vartheta + g_2 \Delta\vartheta^2 + g_3 \left\{ \ln \left(\frac{\vartheta^2 + g_4^2}{1 + g_4^2} \right) - \frac{2\vartheta}{g_4} \left[\arctan \left(\frac{\vartheta}{g_4} \right) - \arctan \left(\frac{1}{g_4} \right) \right] \right\} \\ & + g_5 \left\{ \ln \left(\frac{\vartheta^2 + g_6^2}{1 + g_6^2} \right) - \frac{2\vartheta}{g_6} \left[\arctan \left(\frac{\vartheta}{g_6} \right) - \arctan \left(\frac{1}{g_6} \right) \right] \right\} \\ & + g_7 \Delta\pi [e^{f\alpha(\vartheta)} + K(\vartheta)g_8] \\ & + g_9 K(\vartheta) [(\pi + g_{10})^{(n-1)/n} - (1 + g_{10})^{(n-1)/n}] \end{aligned} \quad (6)$$

where T_0 is a reference temperature set equal to 150 K and $\vartheta = T/T_0$. Eq. (6) uses 23 adjustable parameters that are fitted to experimental data.

40.2.1.1.2 Fluid Equations of State

Based on the pioneering work of van der Waals, cubic EoS represent an important family of EoS with the most well-known being SRK and PR. The equations are used for the calculation of pure component thermodynamic properties and can be extended to mixtures with the introduction of suitable mixing rules. In this work, the van der Waals

one fluid theory (vdW1f) mixing rules were applied using one temperature-independent binary interaction parameter (BIP), k_{ij} , which allows for reliable extrapolation over a wide temperature range. The SFE calculation was also performed using the PC-SAFT [16] EoS, which is a model based on rigorous perturbation theory. In PC-SAFT framework, the Helmholtz energy of a fluid is described as the sum of the Helmholtz energy of a simple reference fluid which is known accurately and a perturbation term. This way, PC-SAFT EoS is written as summation of residual Helmholtz energy (A^{res}) terms that contribute to different molecular interactions. In PC-SAFT, mixing rules are needed for the dispersion interactions and the ones derived from the vdW1f theory were used, coupled with the Lorentz–Berthelot combining rules. A temperature independent BIP was used in this EoS also, in the combining rule for the energy parameter.

40.2.1.1.3 Methodology

Correlation of the pure CO₂ solid-liquid (SLE) and solid-vapor (SVE) equilibrium was the first step in assessing the performance of every combined model and the agreement between them. Moreover, accurately describing the SFE of pure CO₂ is prerequisite for successful two phase and three phase solid-liquid-gas (SLGE) equilibrium mixture calculations.

40.2.1.1.4 Main Research Outcomes

Figure 3 presents the modeling results for pure CO₂ SVE with the three different solid models, when PC-SAFT is used for the vapor phase fugacities and properties calculation. The empirical correlation and the Jager – PCSAFT models are in excellent agreement with each other whereas the thermodynamic integration model deviates at higher temperatures. The same calculations were performed for the SLE of pure CO₂ and results are presented in Figure 4. In this case, all models are in excellent agreement at low temperatures up to 226 K, but at higher temperatures the Jager – PCSAFT model deviates from the other two which remain in excellent agreement.

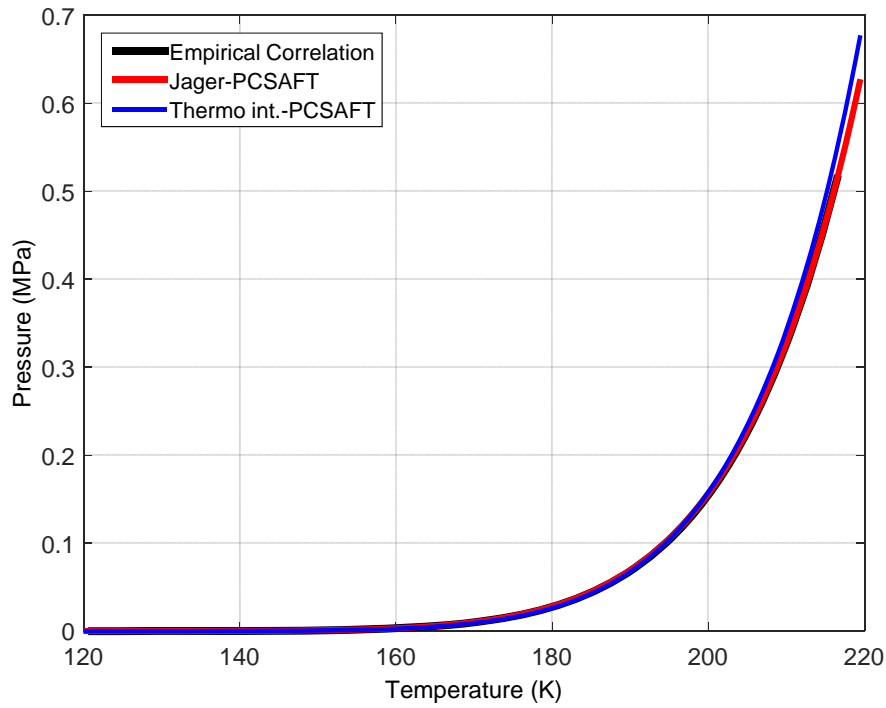


Figure 3. Comparison of Empirical Correlation, Thermodynamic Integration model and Jager and Span EoS, coupled with PC-SAFT EoS for pure CO₂ SVE.

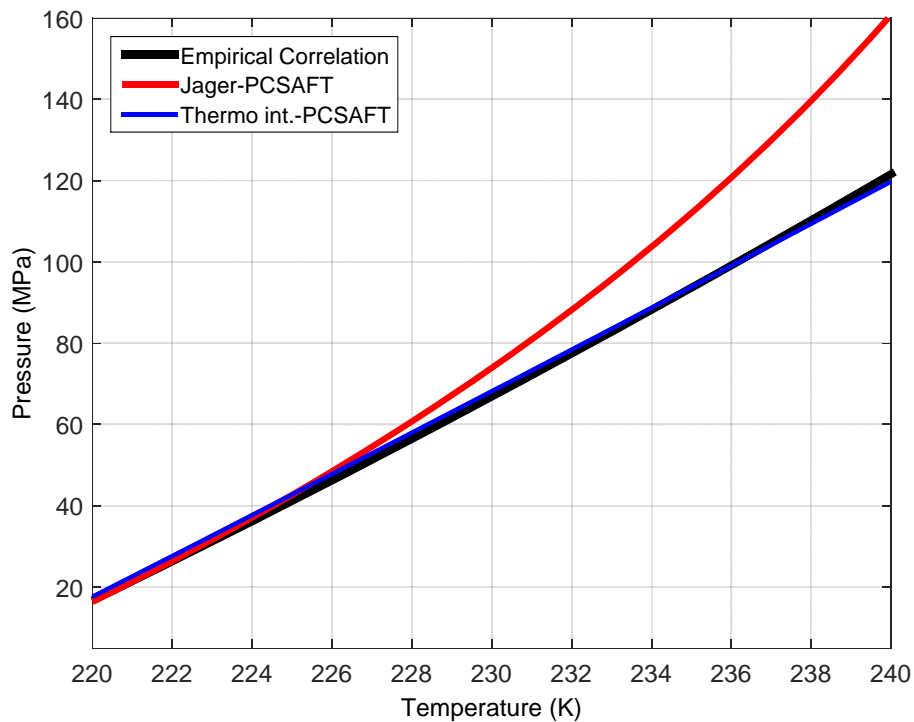


Figure 4. Comparison of Empirical Correlation, Thermodynamic Integration model and Jager and Span EoS, coupled with PC-SAFT EoS for pure CO₂ SLE.

Because of lack of experimental data for the two phase SFE for the CO₂ mixtures of

interest, we evaluated the performance of the various combined models on SLGE conditions and compared to experimental data available in the literature [17-19].

Application of the combined solid-fluid models on the mixtures of interest in this work revealed that an accurate prediction of the SLG mixture locus requires successful reproduction of the pure CO₂ triple point. In general, when all BIPs are set equal to zero, the thermodynamic integration model and the Jager and Span EoS are more accurate in predicting the SLGE for the mixtures of CO₂ with N₂ and H₂, when compared to the empirical correlation model. Combining this solid model with PC-SAFT EoS improves the modeling results, because the reproduction of pure CO₂ triple point is also improved. The use of BIPs, regressed from binary VLE data, significantly improves the prediction of the SLG behavior for most models. Very good behavior with all models is observed for the CO₂ – CH₄ mixture and the use of BIPs led to very low deviations from experimental data. Representative experimental data and model calculations are shown in Figures 5, 6 and 7 for the three CO₂ mixtures.

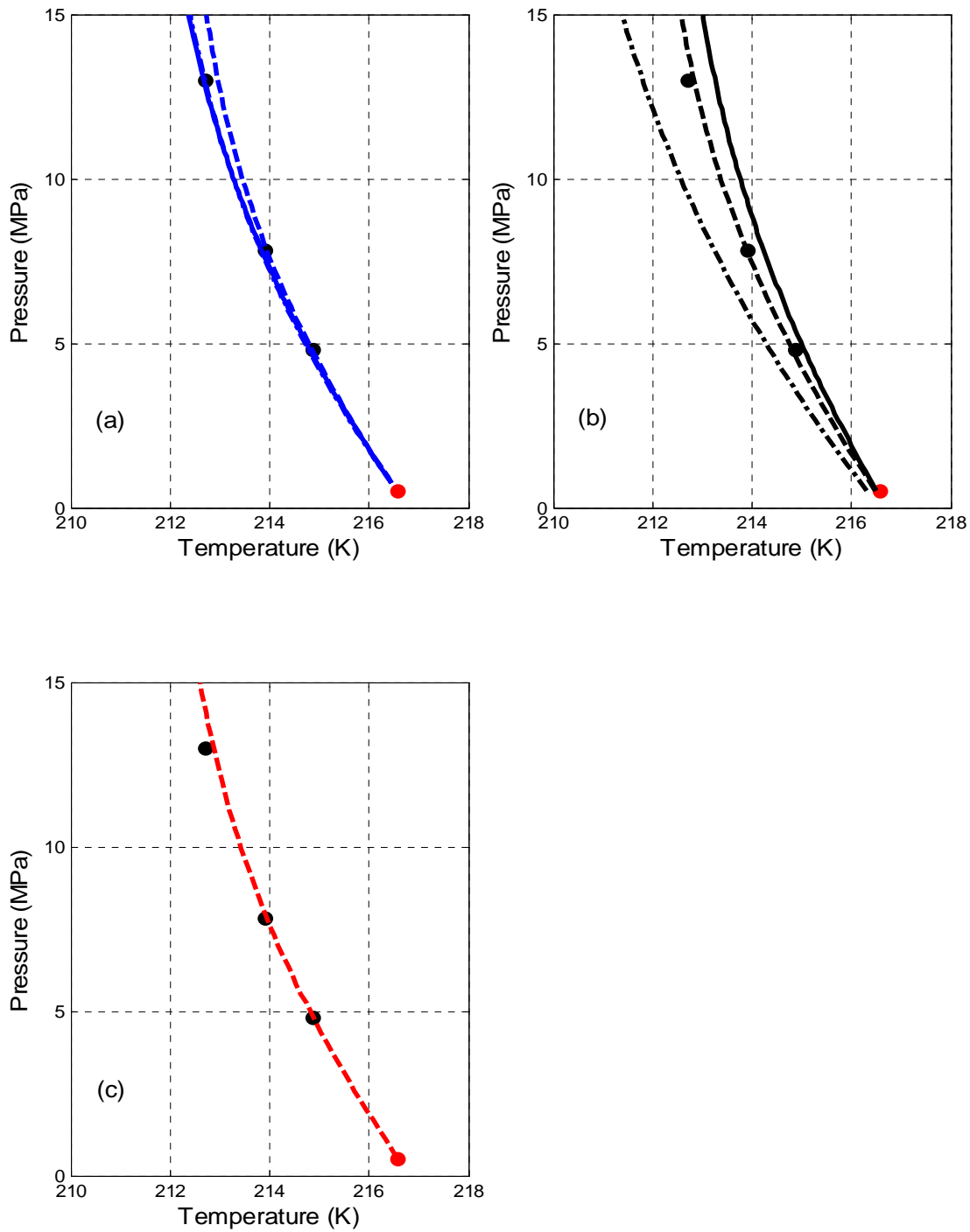


Figure 5. Prediction of the SLG equilibrium curve of the CO₂ - N₂ system with k_{ij} parameters fitted to experimental binary VLE data at low temperature. Results with three different solid models, (a) Thermodynamic Integration model, (b) Empirical Correlation model, (c) Jager and Span EoS, coupled with three fluid EoS. Experimental data [17] are represented by data points and calculations are represented by lines: (—) SRK, (- · -) PR, (- - -) PC-SAFT.

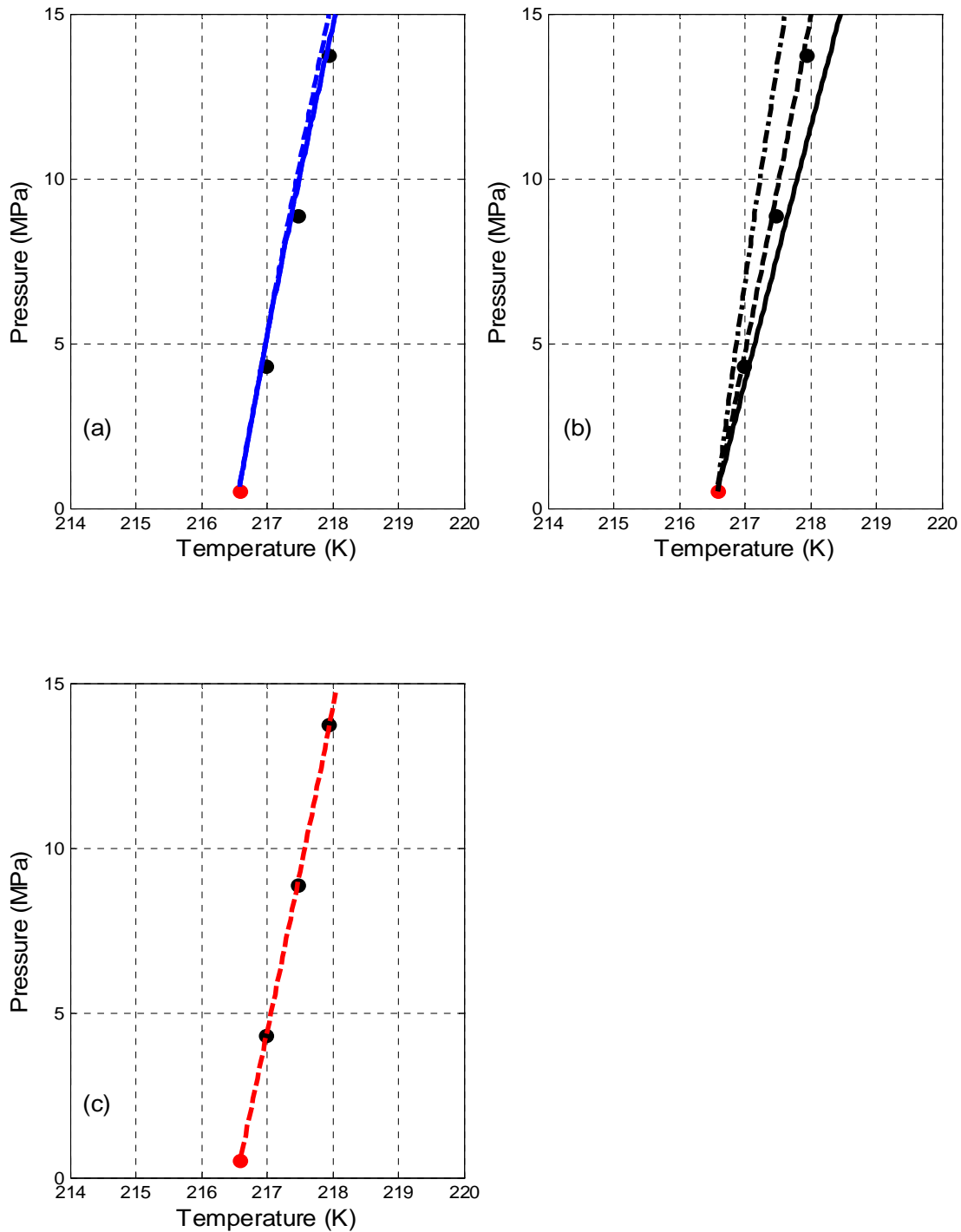


Figure 6. Prediction of the SLG equilibrium curve of the $\text{CO}_2 - \text{H}_2$ system with k_{ij} parameters fitted to experimental binary VLE data at low temperature. Results with three different solid models, (a) Thermodynamic Integration model, (b) Empirical Correlation model, (c) Jager and Span EoS, coupled with three fluid EoS. Experimental data [13] are represented by data points and calculations are represented by lines: (—) SRK, (— · —) PR, (— — —) PC-SAFT.

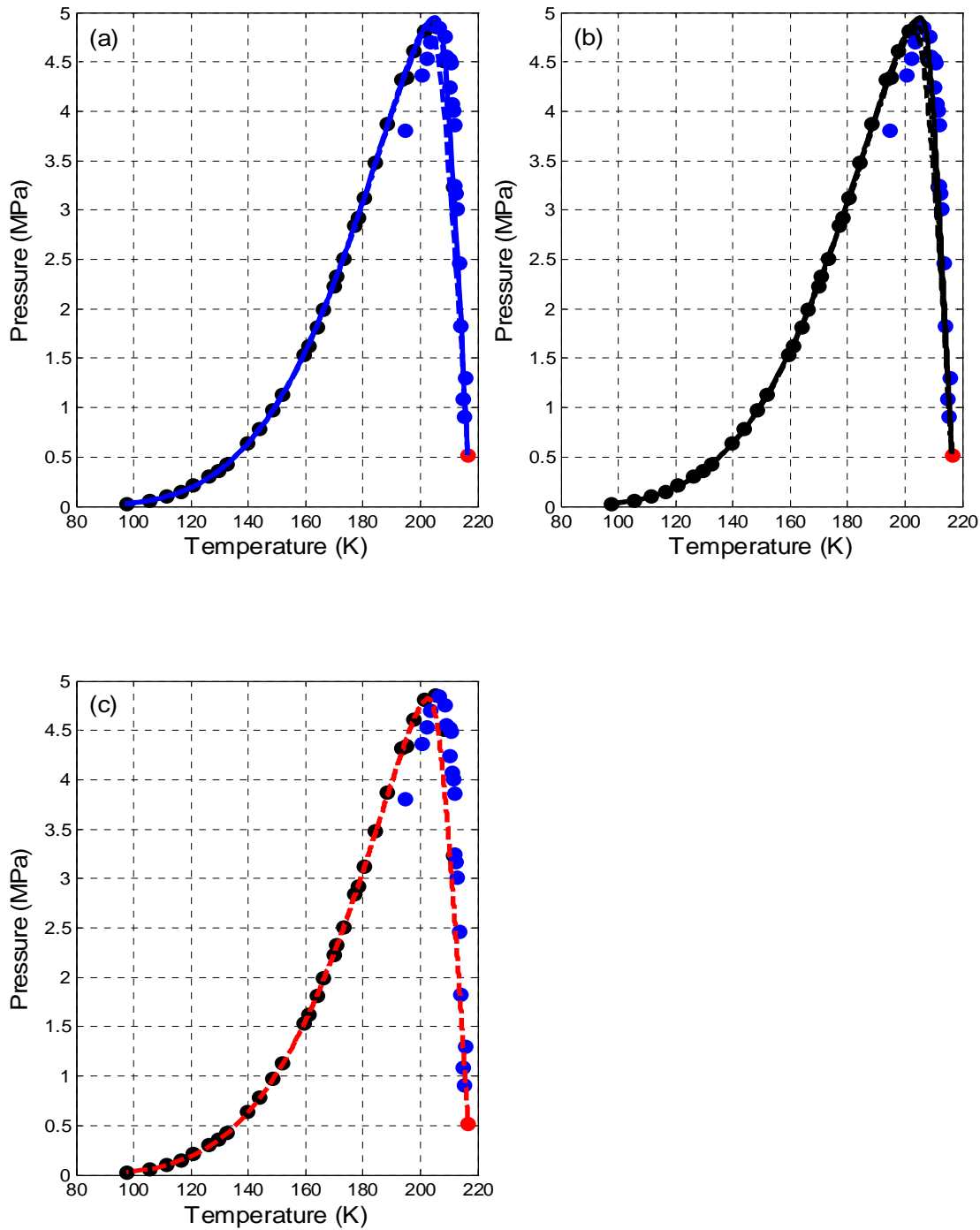


Figure 7. Prediction of the SLG equilibrium curve of the CO₂ – CH₄ system with k_{ij} parameters fitted to experimental binary VLE data from Diamantonis et al. [20] Results with three different solid models, (a) Thermodynamic Integration model, (b) Empirical Correlation model, (c) Jager and Span EoS, coupled with three fluid EoS. Experimental data [18,19] are represented by data points and calculations are represented by lines: (—) SRK, (– · –) PR, (– – –) PC-SAFT.

40.2.1.2 WP1.3 – Experimental evaluation of physical properties of CO₂ mixtures

In this work package we identify the gaps in current knowledge, and guide the experimental programme for physical properties measurements of CO₂ mixtures with impurities at CCS conditions. Experiments have been performed to generate Vapour Liquid Equilibrium (VLE) data for the binary, ternary and multi-component mixtures of CO₂ with impurities. A further set of experiments has been performed to generate data on the transportation properties of CO₂ with impurities. The experimental data is then used to support the development and validation of the EoS in WP1.2.

VLE & Transport Properties Measurement

Work on the thermophysical properties of CO₂ mixtures has been carried out by CanmetENERGY, located in Regina, Canada. This work supports the development of more accurate EoS for these mixtures. Unfortunately, there is an absence of data for CO₂ mixtures, particularly for quaternary and tertiary mixtures, at the pressure and temperatures typical of CCS processes in the open literature, forcing modellers to use more generic EoS to make predictions about the thermo-physical properties of CO₂ mixtures. Experiments have therefore been conducted to generate data and fill some of the gaps in the available thermophysical properties of CO₂ mixtures.

In this context, experiments are carried out using a unique bench-scale CO₂ pressure cell apparatus (0 – 200 bar and -60 to 150 °C). In brief, the pressure cell assembly consisting of a high pressure view chamber, gas mixing and booster pump assembly, syringe pump, recirculating pump, heating/cooling enclosure, density meter and gas chromatograph (Figure

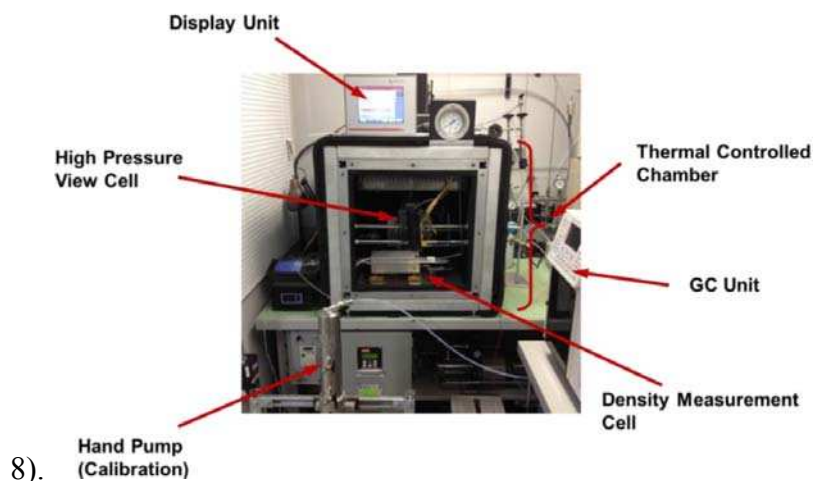


Figure 8. CanmetENERGY's bench-scale CO₂ pressure cell apparatus.

A camera system, situated immediately outside the high pressure view chamber records the phase change of the fluid within the high pressure cell in real time. The novel design for the high pressure view chamber provides the unique opportunity to observe the phase change visually (Figure 9) ensuring the correct sampling is made from either the liquid or vapour.

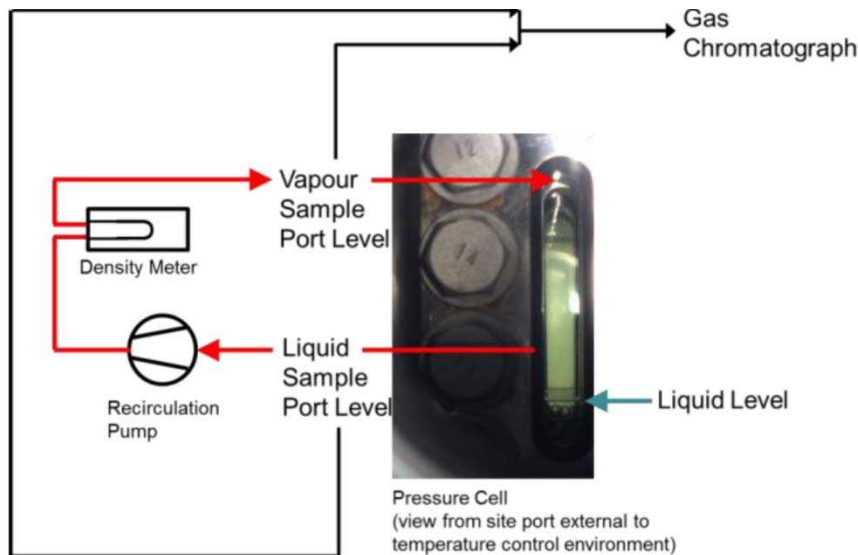


Figure 9. Two phase mixture, as viewed from observation window.

This experimental investigation is focused on the measurement of density and concentration for pressures from 5-80 bar and temperatures from 220-300 K, for a single quaternary mixture and three tertiary mixtures. Testing for the quaternary mixture (CO_2 (93%), O_2 (5.4%), N_2 (1.49%), and Ar (649 ppm)) is ongoing with positive preliminary data at 300 K and 280 K, when compared with estimates from HYSYS. A subsequent snapshot of the density data relative to values from HYSYS are shown in Figure 10.

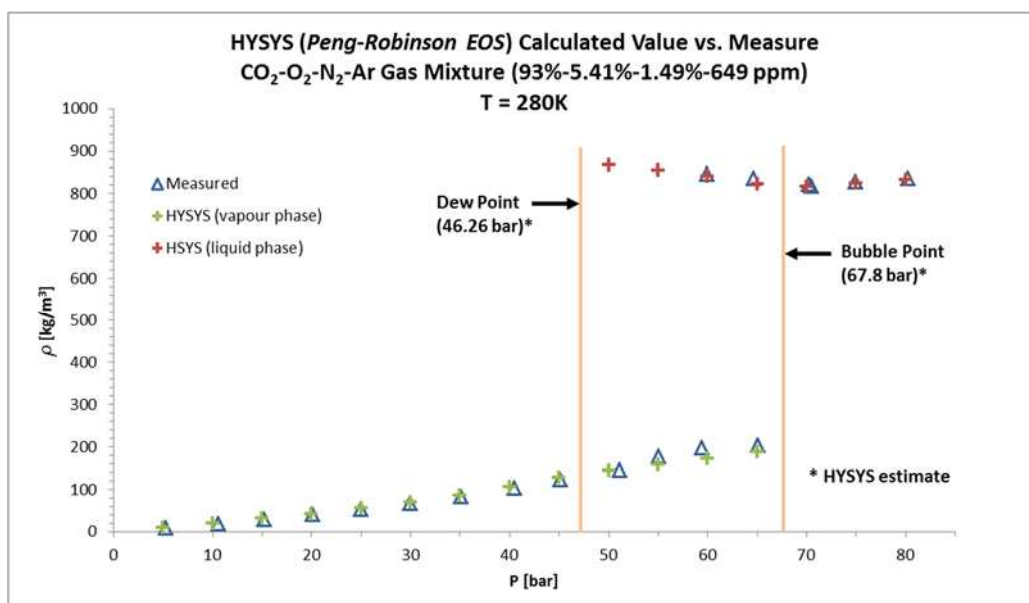


Figure 10. Quaternary gas mixture measured data versus HYSYS calculated values

40.2.2 WP2 – CO₂ Transport

40.2.2.1 WP2.1 – Pressure drop and compressor requirement

In this section non-isothermal steady-state flow has been modelled in order to calculate pressure drop (and hence compressor power requirements) in pipeline networks transporting CO₂ with typical stream impurities using the dedicated EoS developed under WP1. Compression strategies for minimising compressor power requirements have been developed. We have also performed parametric studies using the flow model developed under (1) to identify the type and composition of stream impurities that have the most adverse impact on the CO₂ pipeline pressure drop, pipeline capacity, fluid phase and compressor power requirements.

Compressor Power Requirements

Minimising the pressure drop and avoiding two-phase flows within CO₂ pipeline networks are essential for reducing compressor power requirements. This is critically important given that the compression penalty for CO₂ capture from coal-fired power plants is estimated to be as high as 12% [21].

Table 3. Compositions of CO₂ mixtures captured from oxy-fuel, pre- and post-combustion technologies, adopted in the present study [23].

| | Oxy-fuel | Pre-combustion | Post-combustion |
|-------------------------------|---------------|----------------|-----------------|
| CO₂ (% v/v) | 81.344 | 98.066 | 99.664 |
| O ₂ | 6.000 | - | 0.0035 |
| N ₂ | 8.500 | 0.0200 | 0.2900 |
| Ar | 4.000 | 0.0180 | 0.0210 |
| NO ₂ | 609.0 | - | 38.800 |
| SO ₂ | 800.0 | 700.00 | 67.100 |
| H ₂ O | 100.0 | 150.00 | 100.00 |
| CO | 50.00 | 1300.0 | 10.000 |
| H ₂ S | - | 1700.0 | - |
| H ₂ | - | 15000 | - |
| CH ₄ | - | 110.00 | - |

In order to evaluate the impact of CO₂ impurities on compressor power requirements, a thermodynamic analysis method is applied to CO₂ streams captured using oxy-fuel, pre-

combustion and post-combustion capture technologies, the compositions of which are detailed in Table 3. The analysis is performed for several methods of compression previously recommended for pure CO₂, including the following options [22]:

- Option A: Using the centrifugal integrally – geared multistage compressors.
- Option B: Using supersonic axial compressors.
- Option C: Using compressors combined with liquefaction followed by pumping.

Figure 11 shows an example of the calculation of thermodynamic paths of multi-stage compression combined with intercooling relative to the phase envelopes for pure and impure CO₂ streams, whilst Figure 12 shows the power consumption for each compression strategy (options A, B and C) for mixtures indicative of all capture technologies.

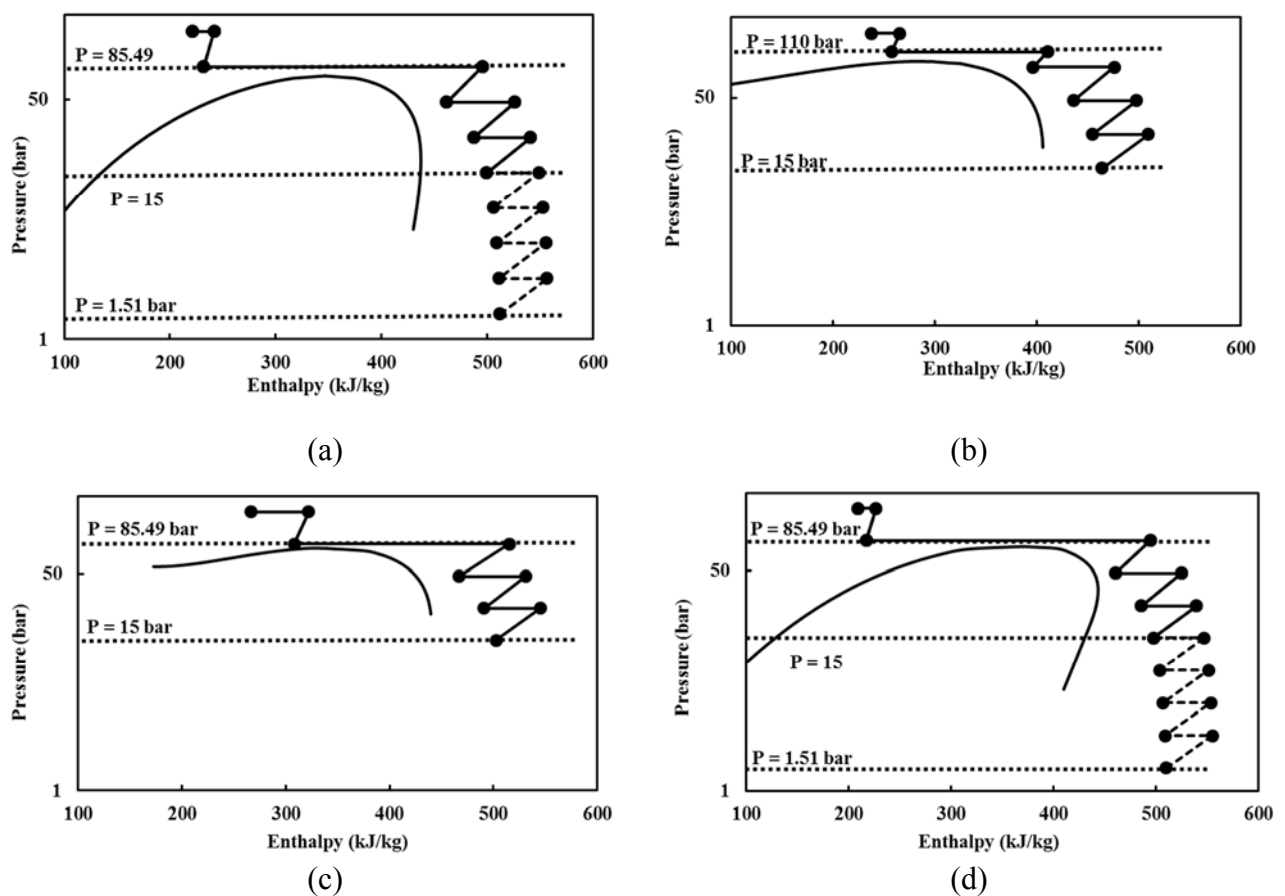


Figure 11. The thermodynamic paths for compression of pure CO₂ (a), and CO₂ mixtures from oxy-fuel (b), pre-combustion (c), and post-combustion (d) capture, using compression and pumping with supercritical liquefaction. Note that the compressor inlet pressure is 1.5 bar for pure CO₂ and post-combustion streams, and 15 bar for the pre-combustion and oxy-fuel streams.

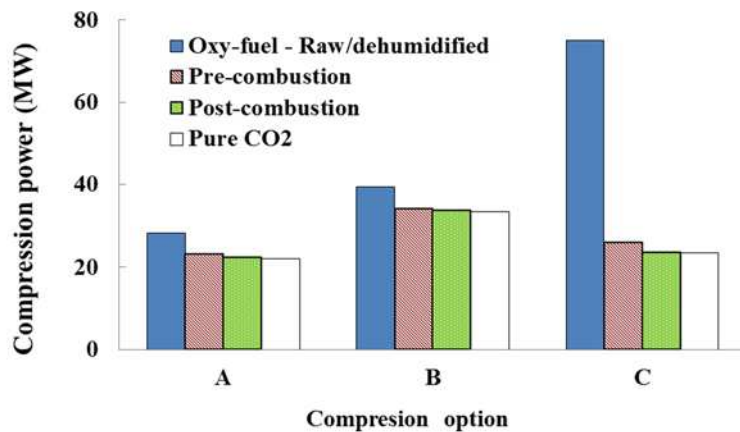


Figure 12. Power demand for high-pressure multistage compression (options A, B and C) of pure CO₂, oxy-fuel (raw/dehumidified), pre- and post-combustion streams (Table 3) from 15 to 151 bar at a capture rate of 156 kg/s.

In particular, Figure 12 shows that in agreement with the data published in the literature, the integration of the multi-stage compression with liquefaction and pumping (Option C) can greatly decrease the total power consumption (combining the power of compression and inter-cooling) when compared to conventional gas-phase compression (Option A). This option is particularly attractive for compression of almost pure CO₂, when liquefaction can be achieved using utility streams at 20 °C for a post-combustion mixture of purity 99.6 vol %, and 8 °C for a pre-combustion mixture (CO₂ purity approximately 98 vol %). At the same time, the cryogenic temperatures needed for liquefaction of oxy-fuel CO₂ streams carrying 74-85 vol% of impurities, may require use of extra power for refrigeration [24]. Clearly, such information forms the foundation for practical optimization of CO₂ compression, which should not be performed in conjunction with other processes involved in the CCS chain, such as the CO₂ capture and transport.

Non-isothermal Steady State Flow Modelling

To evaluate the impact of CO₂ impurities on pressure drop in pipelines, a computer model has been developed that can calculate one-dimensional, transient, compressible, multiphase flows in pipes. This model accounts for both flow and phase-dependent viscous friction, and heat transfer between the transported fluid and the pipeline environment [25-27]. The model has been applied to study the impact of variation in concentration of CO₂ stream impurities at the inlets of a hypothetical pipeline network, upon the pressure and temperature profiles along the pipeline and the delivery composition for a given flow-rates and temperatures of the feed streams [28].

Figure 13 shows an example of the considered realistic pipeline network, transporting CO₂ from Cottam and Drax power stations to the sequestration point at Morecambe South in the East Irish Sea.

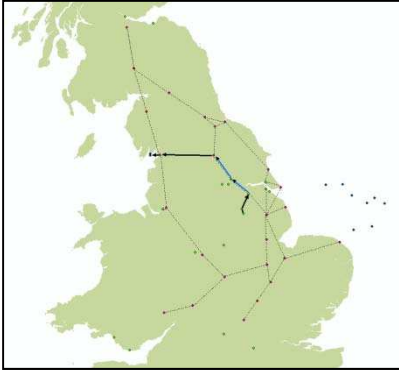


Figure 13. UK CCS network, 2015-2025.

For a pipeline network configuration shown in Figure 13 the analysis of the steady-state pressure drop and temperature profiles has been performed for CO₂ mixtures carrying various impurities, including water, argon, nitrogen and oxygen, which are typically present in the oxy-fuel combustion CO₂ stream.

The model developed can be applied to perform sensitivity studies to identify impurities having the most adverse impact on the CO₂ pipeline transport.

40.2.2.2 WP2.2 – Near-field Dispersion

In this work package, a computational fluid dynamic (CFD) model capable of predicting the near-field structure of high pressure releases of supercritical, dense phase and gaseous CO₂ has been developed. The model is capable of handling CO₂ that contains impurities typical of those to be encountered in an integrated CCS chain, due to it incorporating an equation of state that covers CO₂ with impurities and models for the formation of liquid droplets and solid particles. CO₂ release experiments were performed in order to support this modelling effort. These included controlled small and medium-scale experiments involving high pressure releases of CO₂ with a range of impurities, with near-field measurements of the dispersing jets and pipe-surface temperatures in the vicinity of punctures representative of typical geometries. Another set of experiments were conducted that comprised controlled large-scale experiments involving high pressure releases of CO₂ with a range of impurities, with near-field measurements of the dispersing jets, and temperature measurements in the vicinity of a pre-designed crack geometry. The developed CFD model was then validated

against experimental generated as part of the project described above in addition to data available in the literature. The usefulness of the CFD model developed was then demonstrated by interfacing its predictions for a number of realistic release scenarios with existing far-field dispersion models in order to predict hazards at large distances for use in risk assessments.

40.2.2.2.1 Development of near-field dispersion model

Following the puncture or rupture of a CO₂ pipeline, a gas-liquid droplet mixture or gas alone will be released to atmosphere and disperse over large distances. This may be then followed by gas-solid discharge during the latter stages of pipeline depressurisation due to the significant degree of cooling taking place. The possibility of releases of three-phase mixtures also exists [11]. This sub-section focuses on the detailed mathematical modelling of the near-field characteristics of these complex releases, since predictions of major hazards used in risk assessments are based on the use of near-field source terms that provide input to far-field dispersion models.

Because the pre- to post-expansion pressure ratio resulting from a release will initially be large, the sonic velocity will be reached at the outlet of the pipeline and the resulting free jet will be sonic. This pressure difference leads to a complex shock cell structure within the jet which for the initial highly under-expanded flow will give rise to a flow that contains a Mach disk followed by a series of shock diamonds as it gradually adjusts to ambient conditions. Subsequently, consideration has to be made to the complex physics representing the effects of compressibility upon turbulence generation and destruction. Also, the behaviour of a multi-phase non-ideal system has to be represented by the incorporation of a non-ideal EoS to represent mass-transfer between phases at a range of temperatures and pressures.

Turbulent flow modelling

Descriptions of the numerical approaches to the solution of the fluid dynamics equations applied are presented elsewhere [29], and not repeated here. A modified two-equation turbulence models to represent a compressible system, has also been applied. With respect to two-equation turbulence modelling however, it is now widely accepted that the main contributor to the structural compressibility effects is the pressure-strain term (Π_{ij}) appearing in the transported Reynolds stress equations [30]. Hence, the use of compressible dissipation models is now considered physically inaccurate, although their performance is good.

Ignoring the rapid part of the pressure-strain correlation, Rotta [31] models the term as Equation (5) where ε is the dissipation of turbulence kinetic energy, and b_{ij} is the Reynolds stress anisotropy, as defined below:

$$\Pi_{ij} = -C_1 \varepsilon b_{ij} \quad (5)$$

Later, this model was extended [32] to directly incorporate terms arising from compressibility effects as Equation (6):

$$\Pi_{ij} = -C_1 (1 - \beta M_t^2) \varepsilon b_{ij} \quad (6)$$

where βM_t is a function of the turbulent Mach number, vanishing in an incompressible flow.

Prior to this development, Jones and Musonge [33] provide a model to account for the ‘rapid’ element of the correlation. Defining a function for the fourth-rank linear tensor in the strain-containing term with the necessary symmetry properties, they obtain:

$$\begin{aligned} \Pi_{ij} = & -C_1 \varepsilon \left(\frac{\bar{\rho} u_i'' u_j''}{k} - \frac{2}{3} \delta_{ij} \bar{\rho} \right) + C_2 \delta_{ij} \bar{\rho} u_i'' u_j'' \frac{\partial \tilde{u}_k}{\partial x_l} - C_3 P_{ij} + C_4 \bar{\rho} k \left(\frac{\partial \tilde{u}_i}{\partial x_j} + \frac{\partial \tilde{u}_j}{\partial x_i} \right) + C_5 \bar{\rho} u_i'' u_j'' \frac{\partial u_l}{\partial x_l} + \\ & C_6 \left(\bar{\rho} u_k'' u_j'' \frac{\partial}{\partial x_k} (\tilde{u}_k) + \bar{\rho} u_k'' u_i'' \frac{\partial}{\partial x_j} (\tilde{u}_k) \right) + C_7 \bar{\rho} k \delta_{ij} \frac{\partial \tilde{u}_l}{\partial x_l} \end{aligned} \quad (7)$$

where the C_1 term corresponds to the ‘slow’ part as previously defined as Equation (5), is the turbulence kinetic energy, $\bar{\rho}$ the mean density, δ_{ij} the Kroncker delta, and $u'' u''$ and \tilde{u} the Favre-averaged Reynolds stresses and velocity components, respectively.

Defining the gradient and turbulent Mach numbers as:

$$M_g \equiv \frac{sl}{a} \quad \text{and} \quad M_t \equiv \frac{\sqrt{2k}}{a} \quad (8)$$

Gomez and Girimaji [34] introduce corrections to their derivation of Π_{ij} as Equation (6), which is implemented in terms of a modification to Equation (7) in the current work:

$$\Pi_{ij} = -C_1 (M_t) b_{ij} + \sum_k C_k (M_g) T_{ij}^k \quad (10)$$

The turbulent Mach number is the ratio of the magnitude of the velocity fluctuations to the speed of sound, and the dependence of the ‘slow’ part reflects the degree of influence of dilatational fluctuations. The gradient Mach number characterises the shear to acoustic time scales, and its influence upon the ‘rapid’ part corresponds to the fluctuating pressure field which arises due to the presence of the mean velocity gradient.

Figure 14 depicts the application of these turbulence closures to the prediction of centreline axial velocity, normalised by the magnitude at the nozzle exit, for the highly under-expanded air jet studied by Donaldson and Snedeker [35]. Results obtained using the k- ε model and its associated correction attributed to Sarkar, Erlebacher [36] can be seen to conform with observations previously made with respect to the moderately under-expanded air jet. In this case, the initial shock structure is poorly defined by the standard model, and the over-predicted dissipation of these phenomena is considerable by ten nozzle diameters from the jet outflow. The Sarkar modification to the turbulence dissipation goes some way to reducing the

over-prediction up to approximately 15 diameters, but the resolution of the initial shock-laden region remains poor, and the solution subsequently becomes overly dissipative.

The Reynolds stress transport model with the closure of the pressure-strain correlation attributed to Rotta [31] notably improves upon the resolution of the shock region and the prediction of the dissipation of turbulence kinetic energy. The introduction of a compressible element to the ‘slow’ part of the model as discussed by Khlifi and Lili [32] effects an additional increase in peak magnitude predictions in the near field, although has little effect upon the subsequent downstream turbulence dissipation. The application of a model for the ‘rapid’ part of the pressure-strain term [33], incorporated with the simple model of Rotta for the ‘slow’ part proves a significant improvement with respect to predictions of both the shock resolution and the turbulence dissipation. This is again improved upon by the introduction of corrections based upon the turbulent and gradient Mach numbers as outlined by Gomez and Girimaji [34].

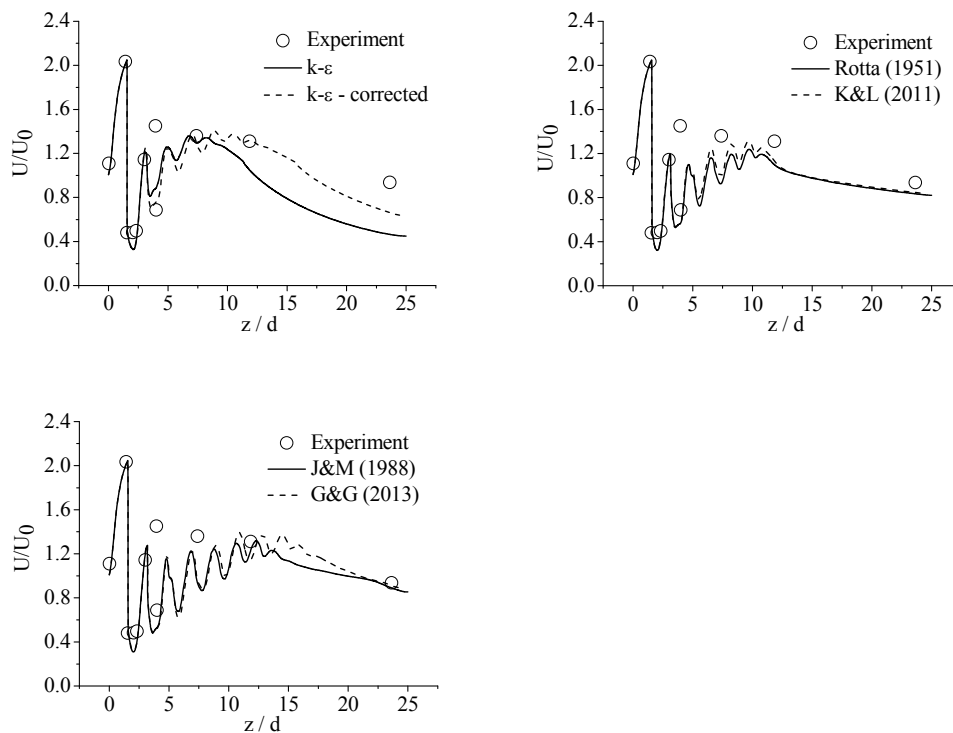


Figure 14. Normalised velocity predictions (top – $k-\epsilon$, middle and bottom – Reynolds stress) plotted against experiment.

Thermodynamics modelling

The Peng-Robinson [36] EoS is satisfactory for modelling the gas phase, but when compared to that of Span and Wagner [37], it is not so for the condensed phase, as demonstrated by Wareing et al. [38]. Furthermore, it is not accurate for the gas pressure below the triple point and, in common with any single equation, it does not account for the discontinuity in properties at the triple point. In particular, there is no latent heat of fusion. A number of

composite EoS have therefore been constructed by the authors for the purpose of comparing performance in application to practical problems of engineering interest. In these, the gas phase is computed from the Peng-Robinson equation of state, and the liquid phase and saturation pressure are calculated from tabulated data generated with the Span and Wagner EoS, or from an advanced model based upon statistical associating fluid theory (SAFT) [14]. Solid phase properties are obtained from an available source of thermodynamic data for CO₂, the Design Institute for Physical Properties (DIPPR) 801 database (<http://www.aiche.org/dippr>), or from a recently developed model attributed to Jäger and Span [39].

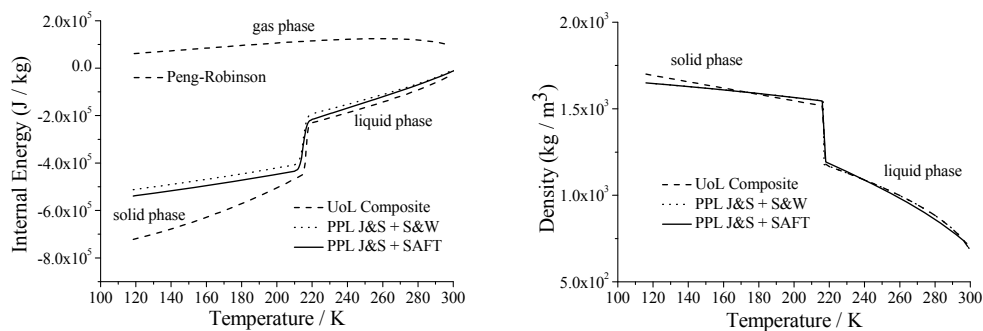


Figure 15. Saturation-line internal energy and density predictions of pure CO₂ using three different equations of state compositions.

Under the remit of the CO₂QUEST FP7 project, the development of a Physical Properties Library (PPL), and hence the provision of a ‘platform’ capable of predicting physical and thermodynamic properties of pure CO₂ and its mixtures, has been undertaken. The PPL contains a collection of models which can be applied regardless of the application, and include a number of cubic formulations such as those described by Peng and Robinson, and Soave, and the formulation of Span and Wagner. Also available is the analytical equation of Yokozeki [40], and the advanced molecular models described as SAFT and PC-SAFT by Gross and Sadowski [16]. A comparative study of the performance of these equations of state has been undertaken using experimental data of high-pressure CO₂ releases for validation. Due to space restrictions, a representative sample of these results is presented which include the composite model described above, and the PPL-derived Jäger and Span [39] model coupled with both Span and Wagner [37] and SAFT. Figure 15 depicts density and internal energy predictions for both the condensed and the gaseous phases on the saturation line for a pure CO₂ system obtained using these three different approaches. Importantly, it can be seen that all models incorporate the latent heat of fusion which must be considered over the liquid-solid phase boundary. They can also be said to similarly represent the internal energy of the liquid phase, although a discrepancy is observed with the composite model. This can be attributed to the inclusion in that model of a small value to ensure conformity with Span and Wagner [37] in terms of the predicted difference between gas and liquid energies [38]. The major discrepancy in predictions lies in the solid-phase region, in that the composite model is in notable disagreement with the models incorporating Jäger and Span [39]. This can be

attributed to the sources of experimental data used in the derivation of the respective models, and the reader is referred to these papers for further information regarding the data sources.

Validation against experimental CO₂ releases

Figure 16 presents sample density and temperature predictions of one of the large-scale test cases used for the validation of the code, obtained using the second-moment turbulence closure [34] and three of the composite equations of state. Undertaken by INERIS, the experimental parameters were a reservoir pressure of 83 bar, an exit nozzle diameter of 12.0×10^{-3} m, and an observed mass flow rate of 7.7 kg s^{-1} . The predictions are of the very near field of the jet, encompassing the nozzle exit, and in the case of the temperature, extending to 0.5 metres downstream. This equates to a distance of approximately 42 nozzle diameters (d), and the Mach disc can clearly be seen as a step-change in temperature just before 0.1 metres. Temperature predictions are in good quantitative agreement with experimental data within this region, although it is difficult to assess how the model performs qualitatively due to the resolution of the temperature measurements available. The difference in predicted solid-phase properties can be seen to influence the temperature predictions most notably in the region 0.02 metres to 0.1 m, where the composite model predicts a warmer jet. Not unexpectedly, this region coincides with the system passing through the triple point at 216.5 K, being notable by the small step-change in the temperature curve of Figure 16, and the subsequent freezing of the liquid CO₂.

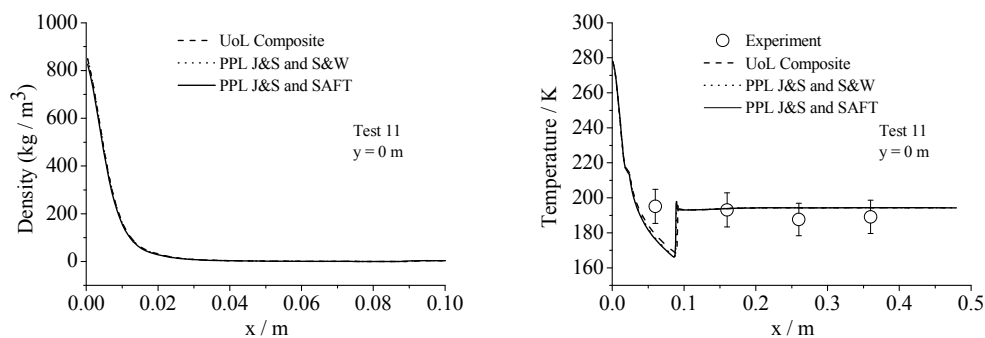


Figure 16. Mean density and temperature predictions of a large scale, sonic release of CO₂ plotted against experimental data.

Density predictions derived from the three models appear to be in good agreement within the very near-field, although closer scrutiny of the predictions reveals the effect of the different solid-phase models. Contrary to intuition, the composite equation predicts a slightly higher density in the first 0.03 metres, but conversely predicts a slightly higher temperature in the region bounded by the triple point and the stationary shock. It is considered that this observation is due to two factors. Initially, the predicted density of the liquid release obtained from this model is greater due to the observed differences in the liquid-phase predictions (Figure 15). Subsequently, as the system passes through the triple point, the composite model

predicts slightly higher temperatures for the solid-phase, which relates to a small correction in the density, bringing them in to line with the PPL-derived models.

Further downstream, and with reference to Figure 17, predictions obtained using the Reynolds-stress model of Gomez and Girimaji [34] and the composite equation of state, are conforming with experimental data both qualitatively and quantitatively, although a slight over-prediction of temperature can be seen across the width of the jet and also with downstream progression. This is indicative of a marginally over-predicted rate of mixing, in-line with previous observations made of the turbulence model validations. It can be said that the second-moment model out-performs the $k-\epsilon$ approach when coupled with the composite equation of state, in that the rate of mixing is better represented. This is manifest as a notable under-prediction of temperatures along the jet axis and also across its width, where the shear layer of the jet is observable as a temperature change of steep gradient, not observed in the Reynolds stress predictions.

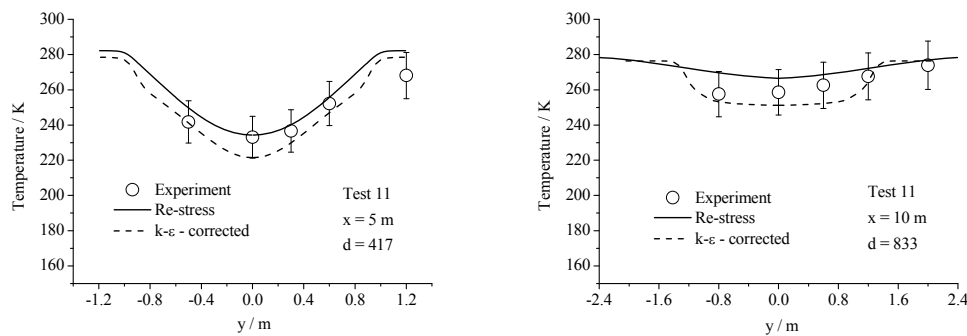


Figure 17. Mean temperature predictions within a large scale, sonic release of CO₂ plotted against experimental data.

Presented are sample results from a number of turbulence and thermodynamics models which have been developed to accurately predict the flow structure and phase behaviour of accidental releases of high-pressure CO₂ for engineering applications. An excellent level of agreement between modelling approaches and experimental data has been observed.

40.2.2.2.2 Medium Scale CO₂ Release Experimental Investigation

Medium-scale experiments involving high pressure releases of CO₂ containing a range of impurities have been conducted at INERIS, France. An experimental rig and techniques developed during the CO₂PipeHaz project [41,42] were used again in order to establish a better understanding of the influence of the presence of impurities on both the flow inside the pipe and on the external dispersion. Measurements in the near-field and in the pipeline outflow allow the further development of databases and will be used for the validation of mathematical models.

The rig and equipment developed in the CO₂PipeHaz project is shown in Figure 18 (Left). This includes a 40 m long, 50 mm internal diameter pipeline, with pressure and temperature transducers placed along the tube at intervals of 10 meters. The near-field is also instrumented with pressure transducers and thermocouples. Equipment has also been especially developed to be adaptable to the study of the 'flash zone' and is shown in Figure 18 (Right).



Figure 18. Left: View of the pipe resting on the weighing masts (blue); Right: near field equipment.

A transparent section is also installed in the centre of the pipe, and the inside flow is visualised during the release with a high speed camera. The pipe is filled via a pump, and the transparent section also permits a check upon the level of liquid CO₂ in the pipe.

A particular focus is made upon the mass flow-rate measurement. To this end, electronic measuring equipment records data at six weighing points. A weighing mast is visible in Figure 18 (Left). Two tests have been run with 100% of CO₂ liquid. The experimental conditions are presented on the next table:

Table 4. Experimental conditions.

| Test n° | | 1 | 2 |
|---------------------|-------|----|----|
| Pressure | [Bar] | 55 | 65 |
| Ambient temperature | [°C] | 18 | 25 |
| Orifice diameter | [mm] | 6 | 12 |

The evolution of the mass versus time, at each measurement point, is presented in Figure 20 for the two tests. Before the release, the total measured mass is not uniform over all measuring points, and ranges from 45 kg to 90 kg. These disparities can be explained by the presence of different equipment on the pipe (measurement, filling, mixing, transparent section).

Figure 19 also presents the evolution of the mass released versus the time. The first period (a few hundred milliseconds after the start of the release) corresponds to the short time during which the fluid inside the pipe is nucleating but appears homogenous. The next period (21 s for test 1 and 5 s for test 2) corresponds to the period where a defined two-phase mixture is present in the pipe and the level of liquid is above the orifice (point U in Figure 19). Subsequently, the level of liquid reaches the orifice (O). After 26 s for test 1 and 11 s for test 2, the level of liquid is below the orifice (D). The two-phase flow ends after less than 2 minutes for test 1 and approximately 25 s for test 2 when the fluid becomes vapour.

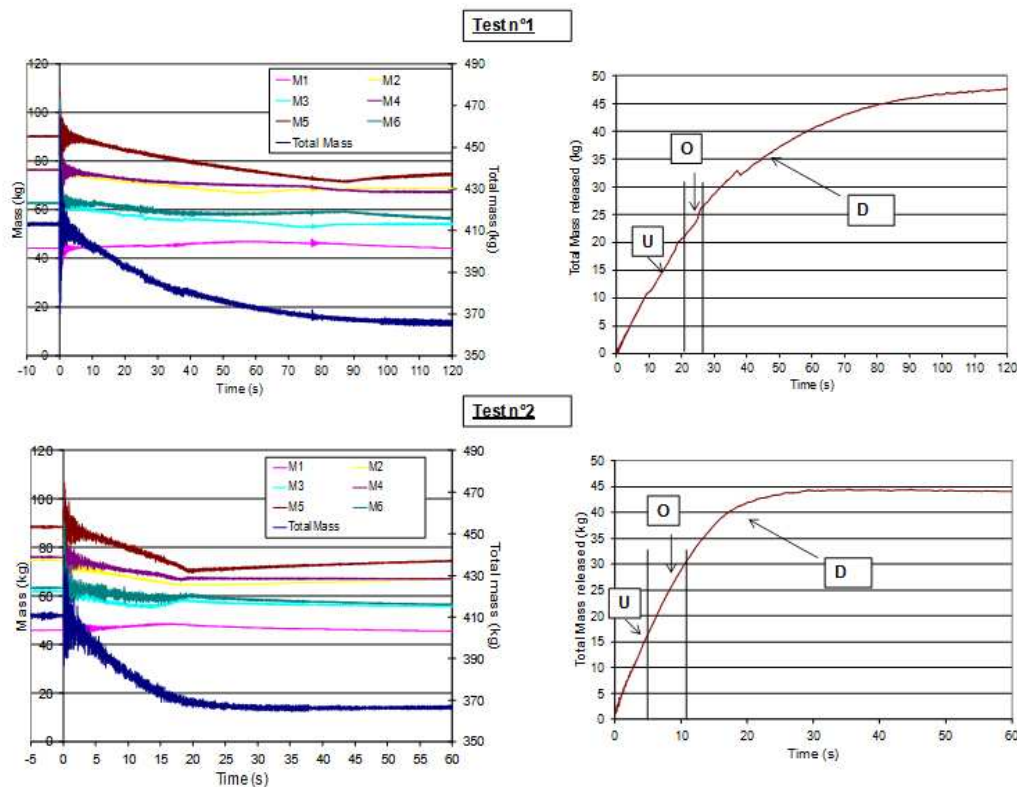


Figure 19. Evolution of total mass, and mass released, versus time.

The mass flow-rate measurement is crucial to the validation of the models [11], and its evolution is calculated by a temporal derivation of the mass released and is presented in Figure 20 for the two-phase flow. The different phases of the releases are identified on the figure depending upon the liquid level in the pipe.

Another issue for modellers is the assumption of adiabaticity. INERIS has added heat-flux meters to the skin of the pipe in order to measure the heat exchanges between it and the

surroundings. An example of the evolution of the heat fluxes are presented for test 2 in Figure 21.

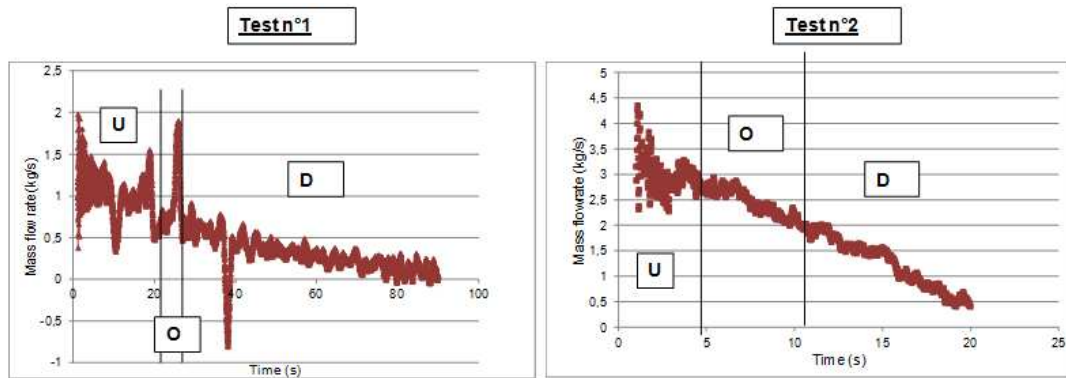


Figure 20. Mass flowrate from the release experiment.

The blue line corresponds to the probe placed on the top of the pipe (gas), and the second probe is located on the bottom (red) corresponding to the liquid.

In addition, insulation has been added to the pipe in order to facilitate the interpretation of the experimental results and assist modellers.

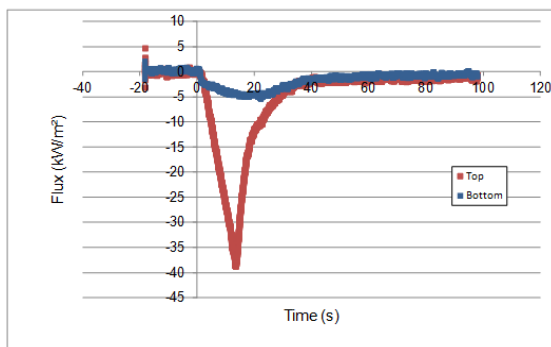


Figure 21. Heat fluxes measured on the top and on the bottom of the pipe.

40.2.2.2.3 Industrial scale pipeline for CO₂ release experiments

Three pure CO₂ release experiments, including one full bore rupture release, have been undertaken using the relocated industrial-scale pipeline in Dalian, China. Impure CO₂ release experiments were also performed in October 2014. The fully instrumented pipeline is 256 m long with a 233 mm inner diameter, and CO₂ temperature measurements were obtained at numerous points in the near field. Photos of the facility and a release experiment are shown in figures 22 – 28.



Figure 22. CO₂ release experimental facility in Dalian, China.



Figure 23. Full-bore rupture release stills with an inventory of 2.43 tonnes pure CO₂ under the following conditions: ambient temperature 36° C, pipeline pressure 52.5 bar, humidity 59 % and CO₂ temperature in the pipeline of 20~30° C.

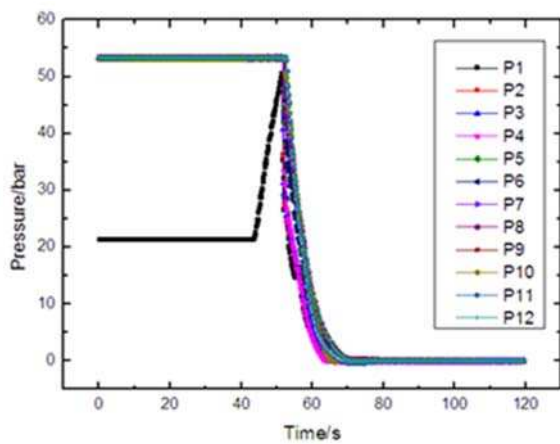


Figure 24. Pressure drop within the pipeline during the full bore rupture release. P1 (release end) to P12 (closed end).

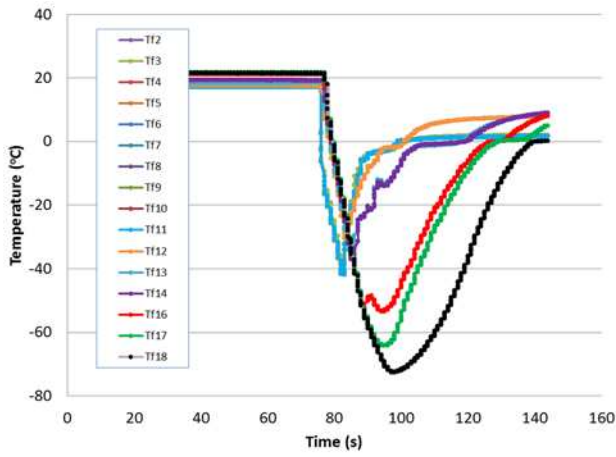


Figure 25. Temperature change along the pipeline during the full-bore release.

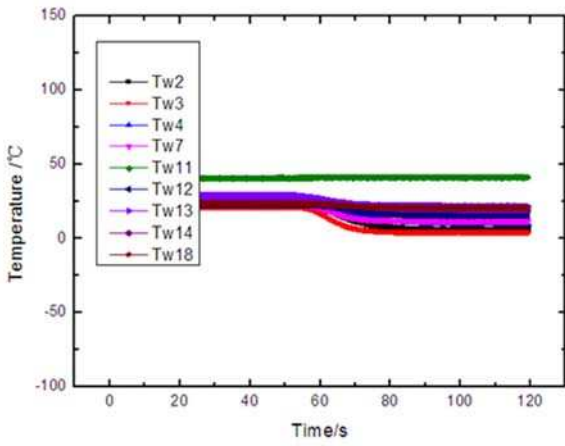


Figure 26. Temperature change of the pipeline wall during the full-bore release.

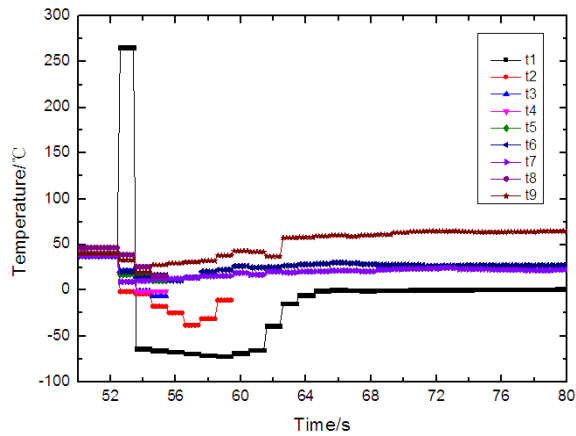


Figure 27. Temperature change in the release near-field during the full-bore release.

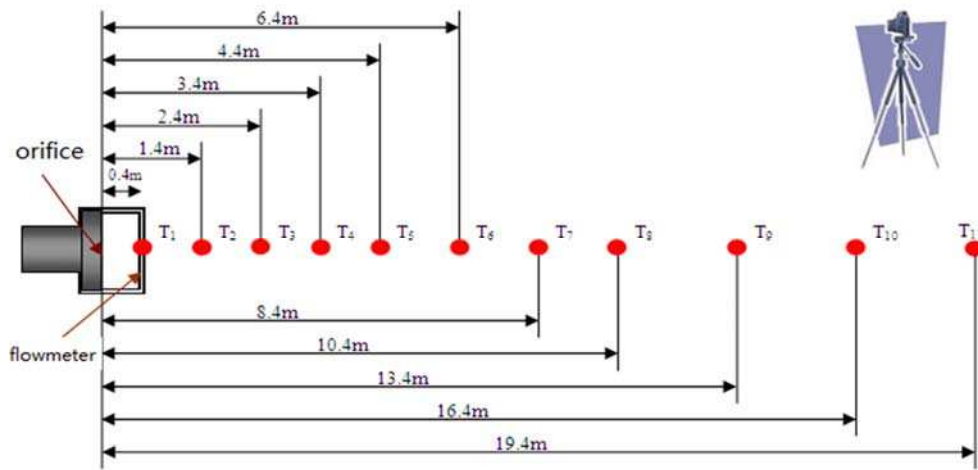


Figure 28. Temperature measurement points in the near field.

The pipeline for industrial scale CO₂ release experiments has a unique design and opening device for controlling CO₂ releases at 80 bar. Full releases are controlled with 2 disk sections with CO₂ or N₂ present between the gaskets. A data acquisition system (pressure and temperature) is installed in the pipeline and operated using LabVIEW with the ability to make measurements of CO₂ and the dispersion area such as the temperature in the near field from the temperature measurement points shown in Figure 28. Over 20 large-scale experimental CO₂ releases including impurities have been conducted using the pipeline providing validation for computational fluid dynamics modelling studies. Experimental measurements from the pipeline including orifice temperature, pressure drop during releases figure 24, pipeline temperature at different locations (figures 25, 26 and 27). Near field CO₂ concentration and decompression behaviour has been investigated using different orifices. The experimental pipeline aims to assist in establishing design standards for CO₂ transportation.

40.2.2.2.4 Ductile and Brittle Pipeline Fractures

In the CO₂QUEST project, ductile fracture propagation behaviour in gas and dense phase CO₂ pipelines made from proposed candidate steels transporting typical stream impurities has been investigated by developing a computationally efficient CFD based fluid/structure interaction model. Sensitivity analyses using the developed fracture model was conducted to identify the type and composition of stream impurities that have the most pronounced impact on ductile fracture propagation behaviour in CO₂ pipelines. Shock tube experiments using the fully instrumented CO₂ pipeline test facility constructed in China were performed to validate the fracture model developed under in addition to pipeline puncture and rupture experiments to validate the outflow model.

A fluid/structure interaction model for brittle fracture propagation in CO₂ pipelines made from the proposed candidate steels transporting typical stream impurities has also been developed. The fracture toughness and crack propagation data of the steel grades has been determined experimentally. The type of impurities and operating conditions that have the most adverse impact on a pipeline's resistance to withstanding long-running fractures for various pipeline steel types have been identified. Prolonged release experiments using the fully instrumented pipeline test facility to validate the model have also been conducted.

Three different steel material grades have been characterised in the CO₂QUEST project, namely X65, X70, and X80. The first two grades are already used in existing CO₂ pipelines, whilst the third grade (X80) is not yet in service. Investigating this material may provide some insights on its usability for CO₂ pipelines. Important aspects for material selection are:

- The response to impurities such as H₂S which may cause sulfide stress cracking.
- Corrosion behaviour: The CO₂ stream is likely to contain impurities affecting the corrosion of pipelines and thus pipeline integrity. Samples of the selected steel grades have been prepared and are being exposed in a lab simulator of another project partner, to a CO₂ gas stream containing typical impurities to investigate the corrosion behaviour experimentally.
- Low temperature behaviour: A leak in a buried CO₂ pipeline can lead to substantial cooling of the surrounding soil lowering the pipe temperature.

To narrow down the material choice and select the most suitable for more detailed investigations, Charpy and Battelle drop weight tear tests were conducted on the three steel grades. The Charpy test results are given in Figure 29 which shows that the X70HIC material had the highest Charpy toughness, and if one takes into account the higher thickness of the test X70 material, it has a similar behaviour in Battelle testing. Since it is also relatively resistant to (accidental) H₂S exposure, the X70HIC was selected for this project as the preferred choice for more in-depth characterization and validation tests.

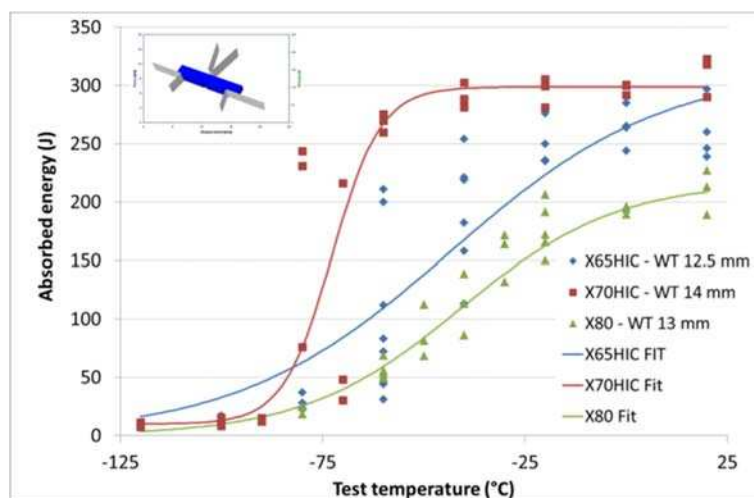


Figure 29. Transition curves for the three materials using Charpy samples.

The actual behaviour of the steel during a CO₂ pipeline failure is not likely to be predictable solely by Charpy and Battelle tests since it also depends on the gas decompression behaviour leading to specific fracture conditions for the material (i.e. temperature, stress concentrations, high deformation speeds, etc.). To tackle this in a universal approach, activities have concentrated upon:

- A numerical strategy to couple the hybrid ductile-brittle damage model used by OCAS to the CFD model of UCL describing the gas decompression [43].
- Improvement of the brittle fracture criterion [44].
- Fine tuning of the parameters of the damage model for the operating conditions typical for CO₂ pipeline failures.

The damage model was not optimally calibrated for high deformation speeds. Therefore, so-called Hopkinson bar experiments were carried out to quantify the material response at strain rates above 500 s⁻¹ which can be observed during crack propagation. Figure 30 compares the fine tune correction function (red solid line) to the old correction function (black solid line).

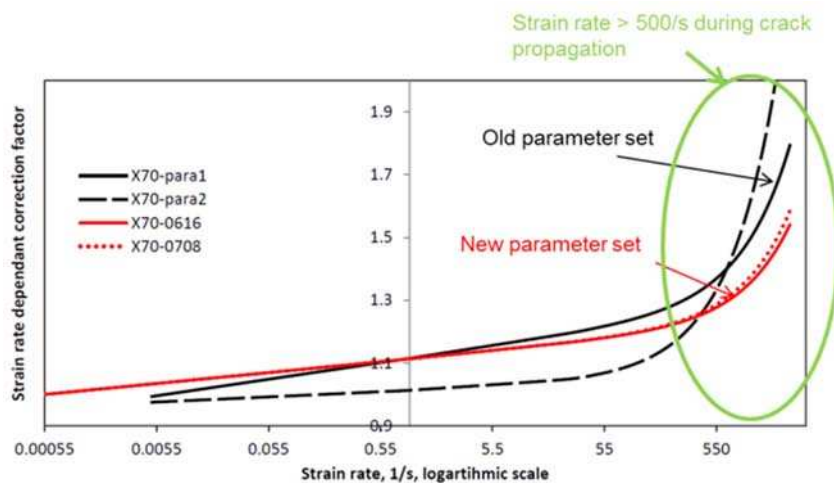


Figure 30. Strain rate dependency in fracture model before and after new Hopkinson bar data.

The brittle fracture criterion has been implemented in the Abaqus damage model. The coupling of this model with the CFD model will be tested and optimised if necessary. Next to this the material and damage model predictions have been validated using medium scale crack propagation experiments and small and medium scale CO₂ release experiments by other partners on components containing an artificial defect.

40.2.3 WP3 – CO₂ Storage Reservoir Performance

In this work package, an understanding of the effects of impurities on the performance of the geological storage operation, in terms of fluid/rock interactions and leakage of trace elements has been developed by means of:

1. A unique field injection test of water and of super-critical CO₂ (with and without impurities, conducted at the experimental site of Heletz, Israel
2. Laboratory experiments aimed at determining the impact of the impurities on the mechanical properties of the reservoir and the caprock

The focus is to use this data to support extensive model development and model application to enhance the understanding of CO₂ geological storage performance in the presence of impurities. The investigation of a potential CO₂ leakage will involve the injection of industrial grade CO₂ into a shallow water aquifer in France, followed by the monitoring the injected fluid, its trace impurities, and the potential mobilisation of metallic trace elements from the rock.

40.2.3.1 Subsurface injection tests of impure CO₂

In this section, laboratory and field scale investigation of the impact of impurities in the CO₂ stream on sub-surface rock properties and CO₂ spreading and trapping behaviour and the subsequent effects on storage performance are described. These experiments have provided unique datasets of field data for model validation. The impact on freshwater aquifers due to possible leakage of trace elements from the injected CO₂ stream has also been investigated and appropriate leakage monitoring methods for such overlying aquifers and at the ground surface have been recommended.

The work by EWRE at the Heletz site, Israel (shown in figure 31) has focused on the configuration of the field experiment aimed at investigating the impact of impurities upon the storage of CO₂. Firstly, major likely impurities emitted with CO₂ from the capture systems were reviewed, and it was suggested to use one with a potential geochemical impact (SO₂) and one with potential physical impact (N₂). Simulations of the behaviour of these impurities upon the reservoir were conducted in order to determine suitable mass fractions that induce a detectable change in the reservoir response. Once the impurities and the mass fractions were known, preparations of the experiment in the field were conducted with the actual procedure for the injection of the impurities with the CO₂ determined. Three options were reviewed: 1) purchasing a prepared mixture of CO₂, N₂, and SO₂, that could be injected directly; 2) conducting the mixing at the wellhead of the injection well; and 3) conducting the mixing at a depth of approximately 1,000 m, as the injection well has an independent connection from the ground surface to this depth.

The field experimental facility consists of two deep wells (1650 m) fully instrumented for monitoring down-hole pressure and temperature, continuous temperature sensing via optical fibre, fluid sampling, fluid abstraction, and CO₂ injection. Design and procurement (or rental) of the equipment needed for the injection of the impurities has been undertaken. The structure of one of the wells is shown in Figure 32.



Figure 31. Aerial photograph of the CO₂ injection site at Heletz, Israel.

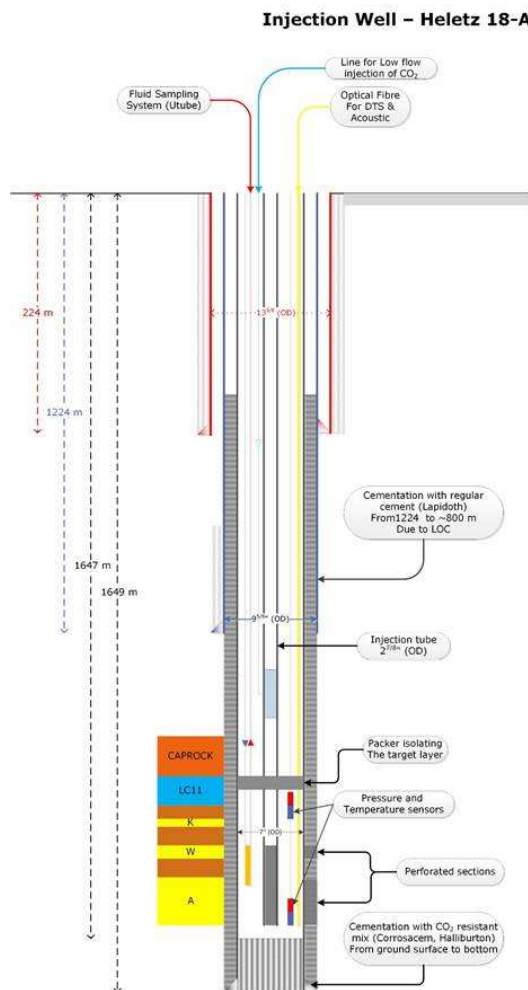


Figure 32. Structure of the injection well at Heletz, Israel.

40.2.3.2 Subsurface hydrological and geochemical modelling

In this section, the theoretical understanding of physical and chemical processes involving impure CO₂ in geological storage is developed, and validated by embedding it within numerical models for simulating CO₂ spreading and trapping and the related coupled thermal-hydrological -chemical processes. In particular:

Through the analysis of laboratory data, in addition to theoretical considerations, the relevant processes and parametric models accounting for the effect of CO₂ impurities CO₂ stream have been further developed and improved upon. Through model application to the region around the injection site as well as on reservoir scale, an understanding of the relevant effects of impurities on storage performance has been obtained.

Geochemical Impact on Impure CO₂ Storage Reservoir Integrity

The presence of impurities within the CO₂ stream might influence physical or chemical properties of a reservoir. In order to enhance the understanding of these changes due to impure CO₂ injection, the critical geochemical impacts on a deep saline aquifer have been modelled using SO₂ as a typical flue gas impurity. Based on geological data of the Heletz saline aquifer situated at a depth of approximately 1600 m [45] a 2D axially-symmetric model was build comprising a total number of cells of 3700 [46]. The grid represents three Lower Cretaceous sandstone layers (thickness from bottom to top 11 m, 1.5 m, and 1.5 m, respectively) with two intercalated shale layers (each with 4 m thickness). Hence, the model covers 18 m in the vertical direction and provides a horizontal extent of 1000 m. Using the coupled thermal-hydrological-chemical program TOUGHREACT V3.0-OMP [47] with the fluid property module ECO2N [48], the SO₂ impurity is introduced as a trace gas within the CO₂ stream with a mole fraction of 97 to 3. This co-injection of CO₂ and SO₂ with a constant rate of 0.28 kg/s takes place at the lower left corner in Figures 33 to 35. The injection period lasted 100 h, representing the planned push-pull test at the Heletz pilot site.

In response to the injected fluid, the native brine is pushed away from the injection point and a distinct dry-out zone evolves, illustrated in high saturation values, i.e. the red area in the vicinity of the injection point in Figure 34. The simulations indicate a preference of flow in the horizontal direction, which is due to a ratio of seven between horizontal and vertical permeability. Both CO₂ and SO₂ injection lower the pH of the initial brine. At the end of the injection period, these changes are detected within horizontal distances of about 18 m in the lowest sandstone layer, whereas in the first overlying shale layer, only the first few meters are affected, see Figure 34.

The strongest impact of SO₂ is related to the fast reacting, pH sensitive carbonate mineral ankerite (CaFe_{0.7}Mg_{0.3}(CO₃)₂). The dissolution of this primary mineral resulting in a release

of Ca^{2+} leads to the precipitation of anhydrite (CaSO_4). In addition with the precipitation of pyrite (FeS_2), these three mineral alteration processes change the spatial distribution of the sandstone porosity. The quantitative modifications to the porosity assumed to be constant within each layer at the start of the simulation are depicted in Figure 35. For the case presented here, i.e. co-injection of about 100 t CO_2 and SO_2 , after about 10 days there is a porosity decrease in the simulated Carboniferous sandstone reservoir of less than 0.005. This change is about 2.5 % of the initial value of 0.2, which seems relatively small, but considering inhomogeneities and potential reservoirs with lower porosities this effect might have a significant impact on injectivity, hence, on pressure management and storage efficiency. Results are highly dependent on initial mineral composition of the reservoir complex. The simulations endorse site-specific modelling based on thorough compilation of input parameter set, including chemical impacts of impurities within the CO_2 stream. Further details can be found in [47].

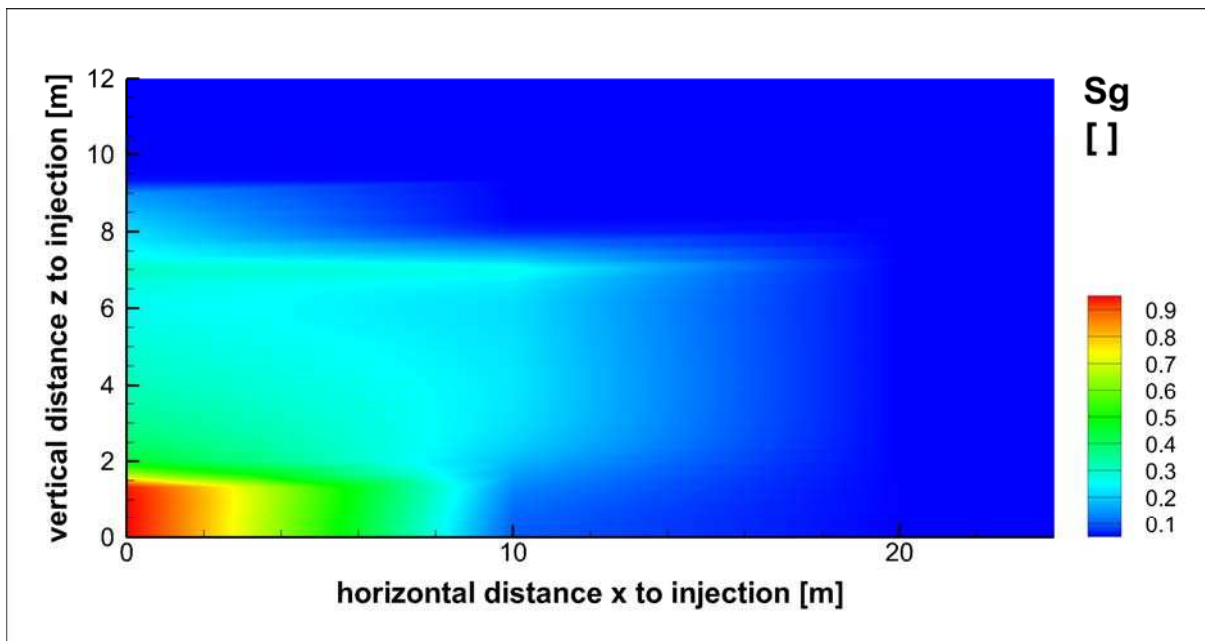


Figure 33. Gas saturation after 10 days of coinjecting about 100 t CO_2 and SO_2 . development of a dry-out zone in the vicinity of the injection point.

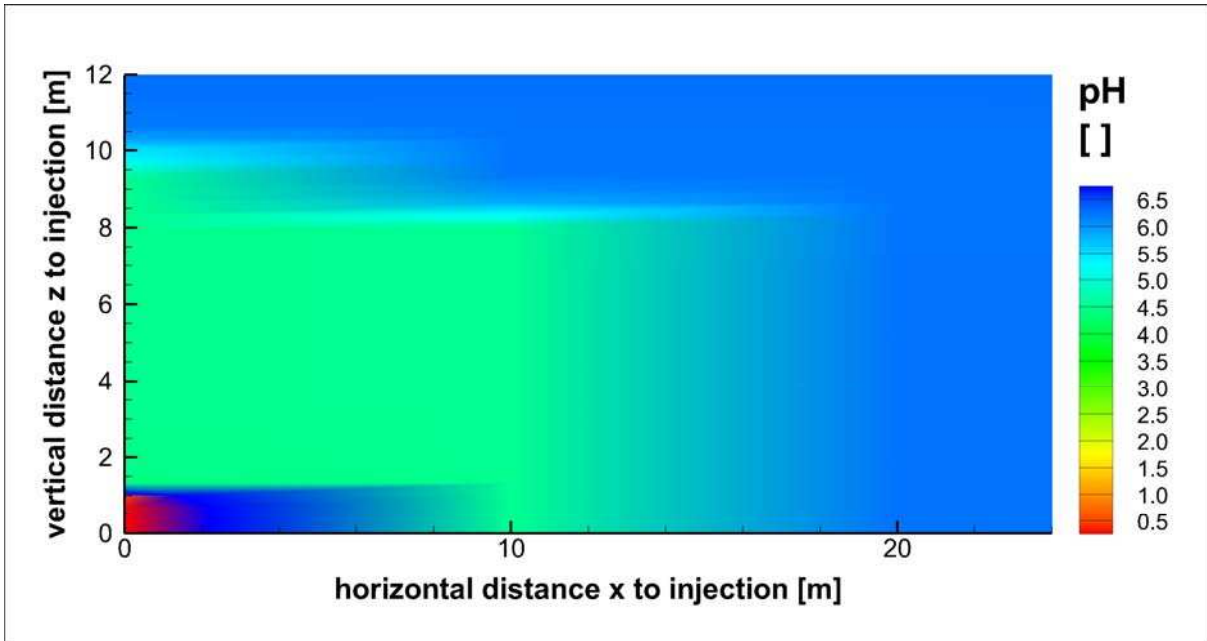


Figure 34. Distribution of pH value after 10 days coinjecting about 100 t CO₂ and SO₂.

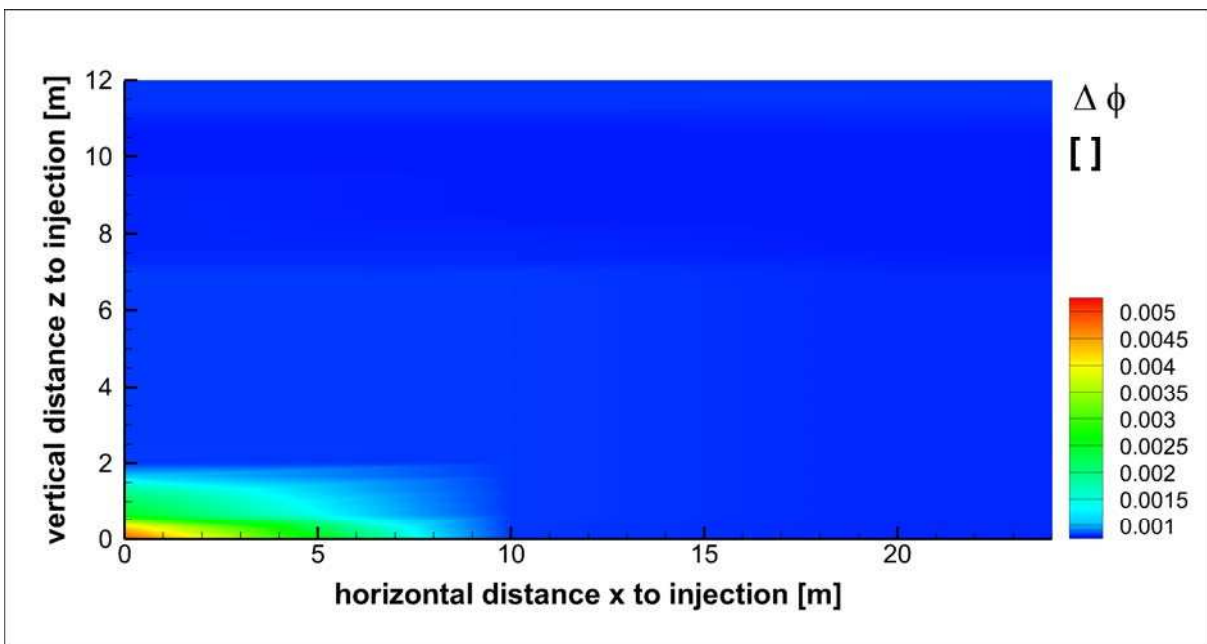


Figure 35. Changes in porosity after 10 days of coinjecting about 100 t CO₂ and SO₂.

40.2.4 WP4 -Techno-Economic Assessment of impurity impacts in CCS systems

In this package, the effect of impurities on CO₂ transport and storage is taken into consideration, in addition to finding ways of blending CO₂ sources and match sources,

transport and sinks. Simulations have been performed to understand the costs and benefits of higher or lower CO₂ purity and generate feasible operational envelopes for CCS systems. Finally, a multi-scale whole systems approach is developed that underpins the overall assessments in CO₂QUEST.

Whole-systems modelling

Imperial College London has applied a multi-scale modelling approach to the analysis of a CO₂ capture and transport system. Focus is upon the development of a series of scale-specific models which interact across a range of length and time scales. This approach is particularly relevant to the CO₂QUEST project as the hour-to-hour behaviour of the CO₂ sources within a given decarbonised bubble will dictate the flow-rate and composition of the CO₂ in the transport network. This modelling approach is illustrated in Figure 36 below.

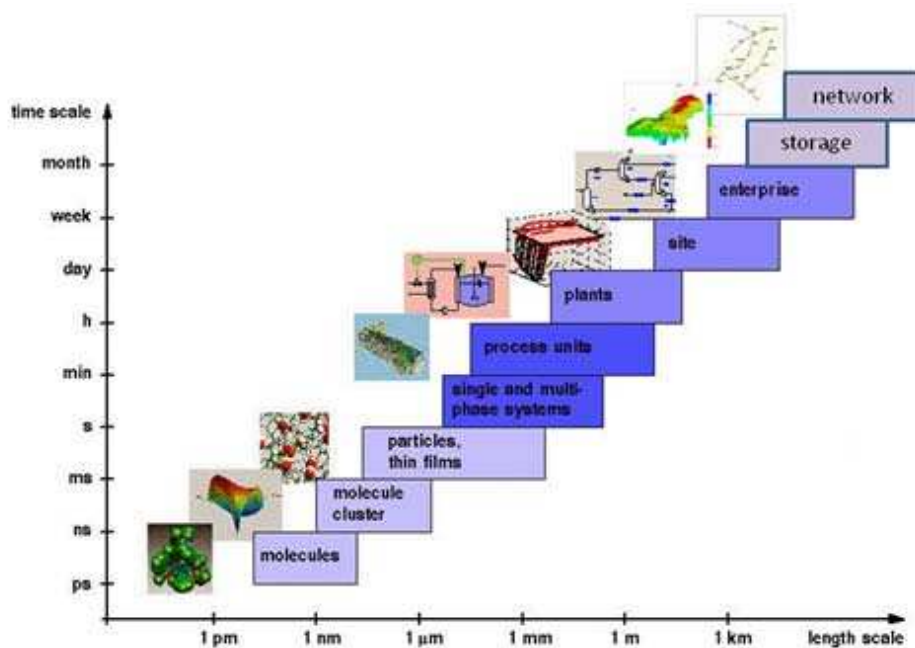


Figure 36. Illustration of multi-scale modelling concept.

As our energy system evolves, incorporating ever greater quantities of intermittent renewable energy, so too will the roles of the various generators which contribute to this system. This is illustrated in Figure 37. As can be seen, as we move from the 2030s to the 2050s and beyond, the role of CCS plants within the energy system significantly changes, and the ability to operate in a flexible, load-following manner becomes more valued.

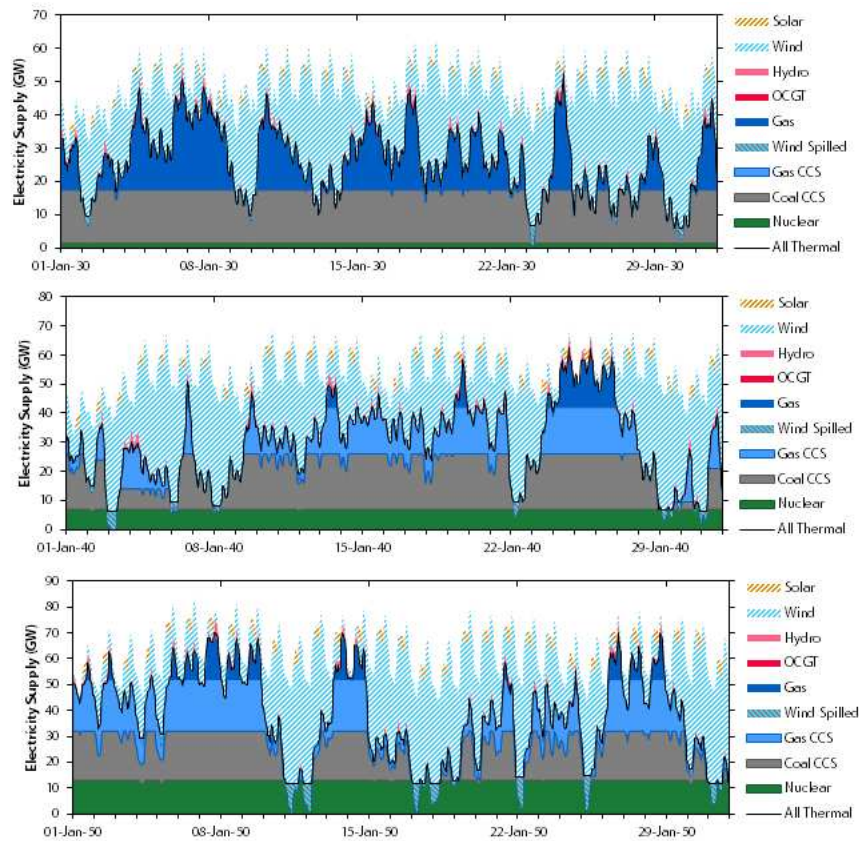


Figure 37. Evolution of operating patterns of the UK power generation system from 2030 to 2050 – output from MESMERISE project using the ETRC model.

In this work, the theory of Grossmann and Sargent [49] has been applied to dynamic, non-equilibrium models of a decarbonized power plant [50-58] and evaluate three distinct options for flexible operation:

1. Solvent storage – a portion of solvent is stored during periods of peak electricity demand and regenerated during off-peak periods.
2. Exhaust gas venting – a portion of the exhaust gas is vented during periods of peak electricity demand.
3. Time-varying solvent regeneration – CO₂ is allowed to accumulate in the working solvent during periods of peak electricity demand and the solvent is more thoroughly regenerated during off-peak periods.

In all cases, a load-following power plant with post-combustion CO₂ capture as a reference case is used. We evaluate each option for flexible operation based upon the Integrated Degree of Capture (IDoC) and cumulative profit realized by the power plant over the course of the simulation. Economic considerations are based on both fuel (coal and gas) prices and a cost of CO₂ emission based on the carbon price floor proposed by the UK's Department of Energy and Climate Change. The time period considered is the early 2030s.

In this section, the results of our optimization problem are presented. For all scenarios, the optimization problem solved was the maximization of profit subject to the end point constraint of the IDoC being greater than or equal to 90 %.

Load-following

This was our benchmark scenario. Here, the capture plant was designed and the operating parameters specified via a steady state optimization as described in our previous paper [57]. We evaluated the effect of a multi-period dynamic optimization had on the end design of the plant. However, as the duration of the period for which the power plant is operating at full load is long relative to the period for which the power plant is operating at part load, the multi-period design was essentially identical to the steady state design, and the solution period of the steady state design problem was an order of magnitude faster than that of the multi-period problem. Thus, in this case, all operating parameters in the CO₂ capture plant, i.e., the L/G ratio, lean loading, ϕ_{lean} , solvent inlet temperature, T_{In}^{Solv} etc., were held constant throughout the simulation.

It can be observed from Figure 38 that, as the capacity factor of the power plant changes, so too does the instantaneous Degree of Capture (DoC), albeit by a very small amount. This is associated with the changing gas and liquid flowrates in the absorption column leading to a variation in the effective surface area in the packed section. This implies that if the duration or frequency of periods of dynamic operation are long or great relative to the duration or frequency of periods of steady state operation, the IDoC could be reduced as a result.

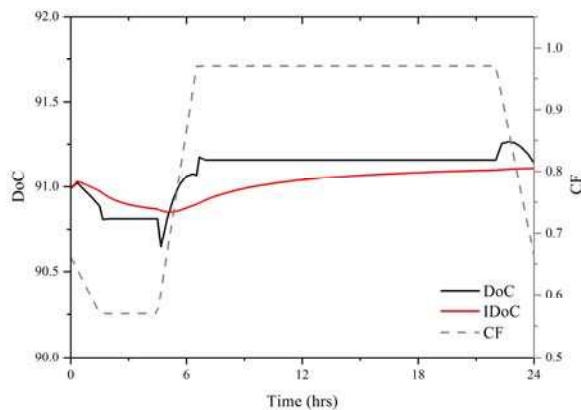


Figure 38. Degree of CO₂ capture varying with power plant Capacity Factor (CF).

As illustrated in Figure 39, an evaluation of the various financial streams associated with the power plant has been provided. It can be observed that the fuel cost per MWh is slightly increased during periods of operation at a low load factor in comparison with periods of operation at a high load factor. This is commensurate with the decreased efficiency of the power plant under this mode of operation. The cost associated with CO₂ emission is similarly

elevated during this period, commensurate with the slightly reduced DoC as illustrated in Figure 31. Finally, as the plant is operating at an essentially constant degree of capture of approximately 90 %, it can be observed that the CO₂ price exerts an important influence on the profitability of the plant.

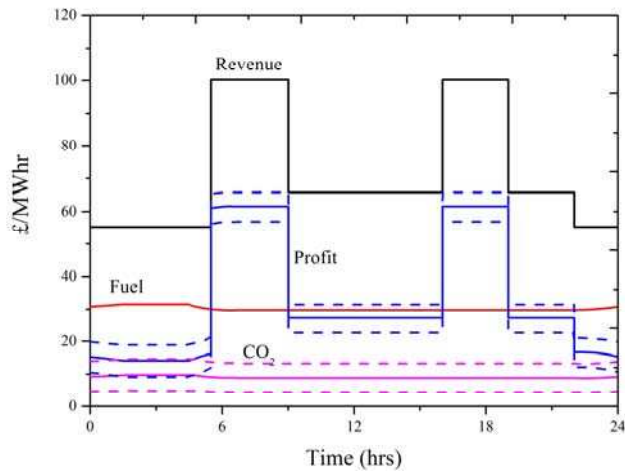


Figure 39. An analysis of the various financial streams associated with the generation of low carbon electricity in the case of conventional load following.

Solvent storage

In this scenario, in order to decouple the operation of the power and capture plants, we consider the option of storing a fraction of the rich solvent during periods of peak electricity prices and subsequent regeneration of the solvent during periods of off-peak electricity prices. Here, the extra parameter to be determined is the quantity of solvent stored or regenerated in each time period. Therefore, this is a multi-period, piece-wise linear, dynamic optimisation problem. As can be observed in Figure 40, when electricity prices are lowest, the flow-rate of solvent to regeneration is greatest. Similarly, during periods of peak electricity price, rich solvent is directed to storage, bypassing the regeneration process.

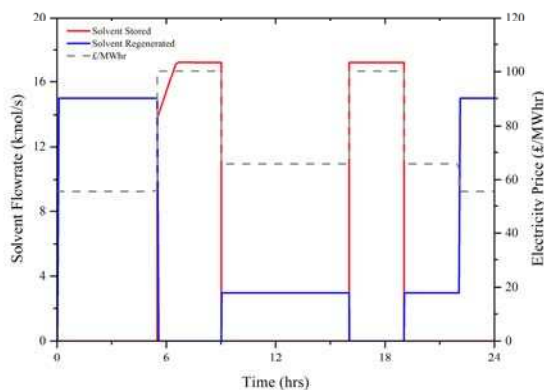


Figure 40. An analysis of the solvent storage and regeneration is presented here.

The advantage of the solvent storage strategy is that it reduces the quantity of steam required for solvent regeneration during key periods of peak electricity demand, as illustrated in Figure 41. However, the availability of steam is a major constraint on the amount of solvent which can be stored during periods of peak electricity demand. It was a constraint in this problem that whatever solvent was stored during periods of peak electricity prices had to be regenerated during off-peak periods. This meant that it was only possible to store approximately 15 % of the total solvent flow. This corresponds to a cumulative volume of stored solvent of approximately 11,750 m³ of solvent over both periods.

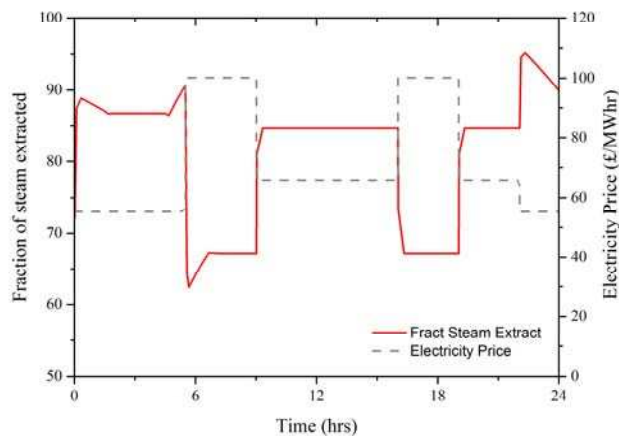


Figure 41. Steam requirement for solvent regeneration under the solvent storage option.

Exhaust gas venting

In this scenario, the power plant ramps up and down, but in order to decouple the operation of the power and capture plants, we consider the option of venting a fraction of the exhaust gas during periods of peak electricity prices. Here, the extra parameter to be determined is the quantity of exhaust gas to be vented in each time period. Therefore, this is a multi-period, piece-wise linear dynamic optimisation problem. The key result of this optimization problem is illustrated in Figure 42 below.

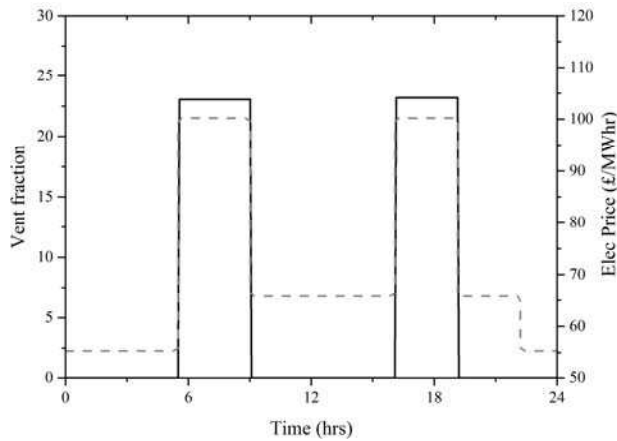


Figure 42. Exhaust gas venting. In this scenario, approximately 23% of the exhaust gas was vented during periods of peak electricity prices.

As can be observed from Figure 42, during periods of peak electricity prices, approximately 23% of the total exhaust gas was vented. In this scenario, we departed from the conventional procedure of capturing 90% of the CO₂ at all times. Rather, of the exhaust gas which was introduced into the absorption column, 95 % of the CO₂ was captured. However, during the periods of exhaust gas venting, the DoC fell to approximately 74 %, increasing the carbon intensity of the electricity generated to approximately 225 kg/MWh. This is illustrated in Figure 43. It is noted that the venting of this quantity of CO₂ had the primary consequence of imposing a significant cost penalty on the profitability of the plant and the secondary consequence that it was not possible to solve the optimization problem with the end-point constraint of IDoC \geq 90 %. Here, this had to be loosened to 89 %.

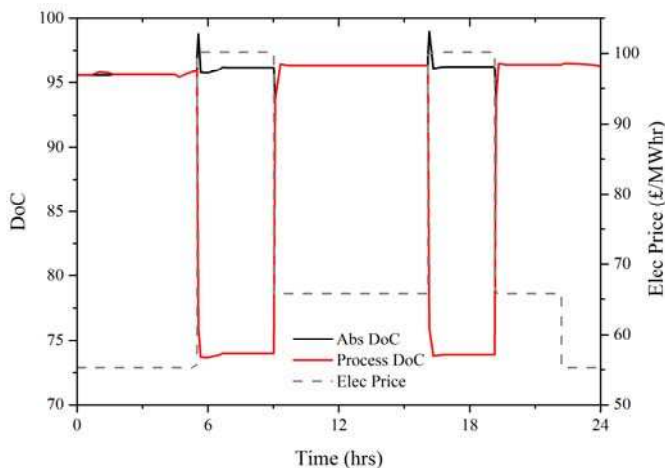


Figure 43. Variation in DoC with exhaust gas venting. It can be observed here that the absorber DoC remains approximately constant.

Time-varying solvent regeneration

In this section, we evaluate the option of using the working solvent as means to provide flexibility to the power plant. This is achieved by allowing the CO₂ to accumulate in the working solvent during hours of peak electricity prices and regenerating the solvent more completely during off peak periods. This is not storing solvent separately to the capture plant; this is storing CO₂ in the solvent which is circulating within the capture plant. This means that the lean loading of the solvent is no longer a time-invariant process parameter. Rather, this control vector is now parameterised such that it is expressed as:

$$\theta_{Lean}^k = \alpha^k t^2 + \beta^k t + \gamma^k \quad (11)$$

Where θ_{Lean}^k is the function describing the way in which θ_{Lean} varies across a given period k , α^k , β^k and γ^k describe this function in each period k , and finally t is the time in each period k . Here, the variable t is the time in each period k and which is set to zero at the beginning of each new period. The only additional constraint we have imposed upon the optimisation problem by this formulation is the quadratic nature of the parameterisation. This could have equally been a cubic or higher order polynomial, however a quadratic polynomial was chosen in the interest of simplicity. Further, we did not constrain the values of the coefficients of this polynomial, i.e., the magnitude of the subsequent behaviour was strictly a function of the process response to the time-varying electricity prices. The results of this optimisation problem are presented in Figure 44.

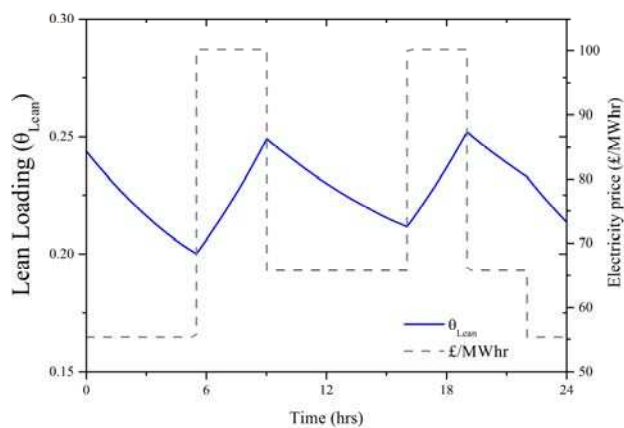


Figure 44. Solvent regeneration as a function of time and electricity price is shown here.

As can be observed, and as opposed to operating at a constant lean loading (the continuous blue curve), the degree of solvent regeneration varies in sympathy with the prevailing electricity price, as might be expected for the solution of this kind of optimisation problem.

The solvent is deeply regenerated during periods of low electricity price, whilst CO₂ is allowed to accumulate in the working solvent volume during periods of high electricity price. This has the effect of allowing the plant to direct substantially less steam to solvent regeneration operations when the opportunity cost associated with doing so is high. Obviously, following this kind of operating strategy will have the effect of varying the carbon intensity of the electricity generated.

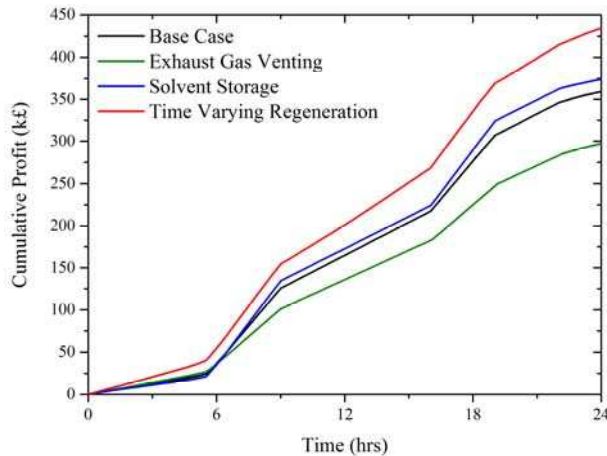


Figure 45. Cumulative profit available for each option.

Finally, it is instructive to consider the profitability of the power plant, which is illustrated in Figure 45. It is apparent that the solvent storage option offers marginally greater profitability (ca. £374k) when compared with the base case (ca. £359.6k), approximately a 4 % improvement, whereas the exhaust gas venting option (ca. £298.6k) is approximately 17 % less profitable than the base case. Finally, the variable solvent regeneration option (£417.5k) is 16 % more profitable than the base case scenario.

40.2.5 WP5 – Impurity Impacts and Risk Assessment

In this package the incremental risks across the chain implied by the presence of impurities in the CCS chain have been explored and defined. A decision making risk assessment method covering both safety and impact on the environment with a particular focus on the role of impurities has been defined. This method has been applied to devise appropriate prevention and mitigation measures for selected risks.

Impact Profiles of Impurities

An additional challenge in the CO₂QUEST project was to identify and assess the incremental risk due to the presence of impurities in a CO₂ stream. A first step towards this objective is to undertake an impact-profile risk-analysis for each part of the CCS chain and each common impurity.

Impacts mechanisms

To date, an overview of the current knowledge regarding the key effects of impurities along the CCS chain has been carried out. This also provides useful input to the design of a risk assessment and environmental analysis methodology, based upon the single and combined impurities effects. The work undertaken is based on a range of impurities identified by WP1 of the CO₂QUEST project. For each impurity, its effects all along the CCS chain are identified via 3 categories of impacts:

1. The physical impacts.
2. The chemical impacts
3. The toxicological and ecotoxicological impacts

Physical impacts

Physical impacts of the impurities contained in captured CO₂ streams are a major concern for two main reasons. Firstly, the impurities responsible for these impacts are very common in the CO₂ streams produced from the main capture technologies (pre-combustion, post-combustion, and oxyfuel combustion). Secondly, the physical behaviour of the CO₂ stream has macroscopic impacts all along the CCS chain. In fact, by reducing the overall efficiency of the CCS application or by improving its global cost, physical effects of impurities could have major consequences, which have to be assessed and forecast. Figure 46 depicts example impact mechanisms.

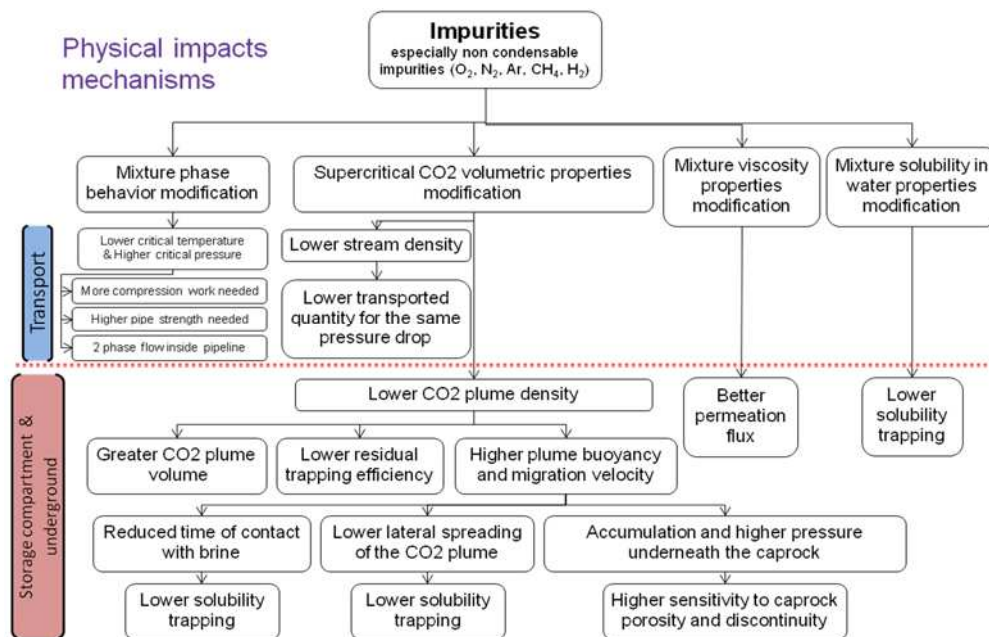


Figure 46. Physical impacts mechanism.

Chemical impacts

During transport and storage, a CO₂ stream experiences a number of different steps and physical conditions that can lead to significant chemical alterations. This alteration of CO₂ properties on a chemical level can instigate unwanted subsequent reactions. Figure 47 highlights some of these possibilities.

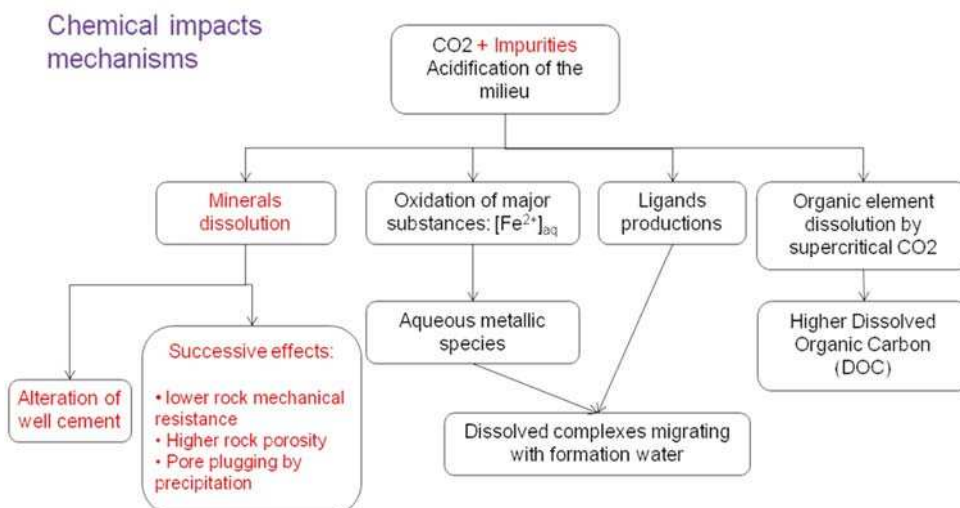


Figure 47. Chemical impacts mechanisms.

Toxical and ecotoxical impacts

Once injected into the storage environment, potential impacts of the CO₂ need to be considered on a long-term scale. Indeed, environmental impacts may still occur in the case of loss of containment. Such a loss can be a result of either an integrity default of the storage (fault through the caprock, existing or well) or too high caprock porosity. Concerning toxicity and environmental sensitivity, even low concentration of impurities may have significant impacts. Figure 48 graphically depicts some of the toxicity mechanisms.

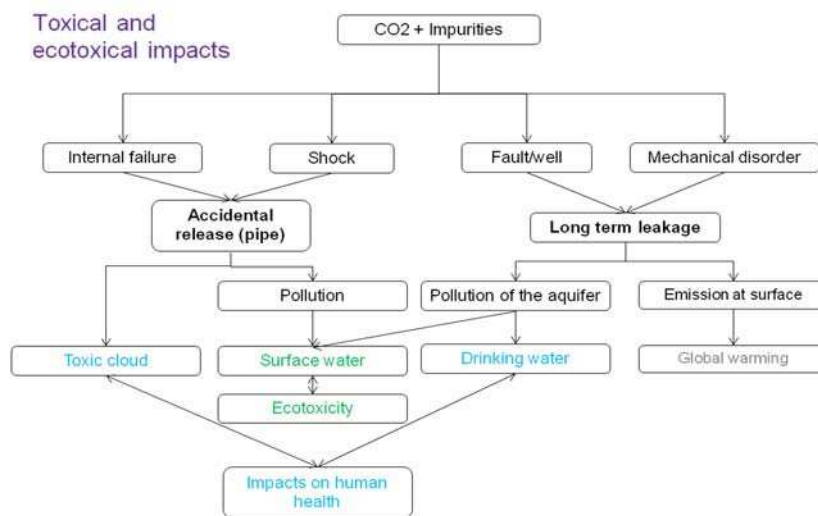


Figure 48. Toxical and ecotoxical mechanisms for CO₂ containing impurities.

Matrix tool

For each impurity identified by other partners as a common impurity, all the potential impacts described above are investigated and displayed in a matrix tool, with the concentration thresholds when relevant. An extract of this matrix tool is presented as Figure 49.

In order to provide an in-depth understanding of the types of phenomena that can occur during accidental releases of high-pressure CO₂, medium and large-scale pipeline rupture experiments incorporating extensive real-time monitoring instrumentation were conducted. In particular, these experiments for the first time elucidated the influence of the presence of impurities on the flow characteristics inside the pipe and hence the near-field and far-field dispersion behaviour of the released CO₂ cloud. The data recorded using these experiments were in turn employed for the validation of the rigorous heterogeneous flow and dispersion models developed for predicting the impact of the various impurities on the discharge behaviour and hence the minimum safe distances.

Investigations of three different steel materials for pipelines were conducted to establish their sensitivities to CO₂ impurities on their corrosion behaviour and susceptibility to brittle and ductile fracture propagation. The fracture studies were complimented with the development of fully predictive fluid/structure models coupling finite element analysis and the CFD flow model to predict the pipeline fracture toughness required in order to resist running fractures.

WP3 was devoted to developing understanding of the impacts of impurities in the subsurface during geological storage of CO₂. The results of CO₂ mixture injection experiments in close proximity to a shallow aquifer indicated no measureable cross-over contamination of the water table by the CO₂ impurities. The deep well CO₂ mixture injection experiments investigating fluid/rock interactions have been highly challenging and still ongoing.

The geochemical impact of impure CO₂ on storage reservoir integrity in a deep saline aquifer has also been studied through modelling. An axially-symmetric 2D model was constructed to simulate the relevant reactive transport models focussing on the impact of SO₂ on the brine-rock system in sandstone, showing the acidic and reactive properties of this impurity.

WP4 focused on full-chain CCS techno-economic analysis of CCS networks, which included detailed process system simulation of different options for CO₂ purification from oxyfuel combustion and post-combustion capture technologies. The different product purities for the different CO₂ captures were taken into consideration when modelling the CO₂ transport networks, blending CO₂ streams from various sources into a trunk pipeline with a CO₂ stream of composition suitable for subsurface injection. Finally, the optimised overall CAPEX and OPEX of the full chain system was derived for the anticipated ranges of CO₂ purity for the different sources.

WP5 analysed the downstream impacts of CO₂ impurities on pipeline transport and geological storage by classifying impurity impacts into physical, chemical and toxic, and by developing a point scoring mechanism to describe their severity.

In conclusion, the CO₂QUEST project has led to the development of rigorous validated theoretical modelling tools [12,27,28,43,56] complimented with the state of the art-experimentation [41,42] to determine the optimum level of CO₂ purification required in order to enable the design of safe and economic CCS technologies.

40.4 Acknowledgments

The research leading to the results contained in this chapter received funding from the European Commission 7th Framework Programme FP7-ENERGY-2012-1 under grant number 309102. The chapter reflects only the authors' views and the European Commission is not liable for any use that may be made of the information contained therein. A few text excerpts are taken from the CO₂QUEST newsletter Autumn 2014 [52].

40.5 References

- [1] J. Serpa, J. Morbee, E. Tzimas, Technical and Economic Characteristics of a CO₂ Transmission Pipeline Infrastructure, in, Joint Research Centre Institute for Energy, Petten, 2011.
- [2] CO₂QUEST, 2013. Impact of the Quality of CO₂ on Storage and Transport, CO₂QUEST Project Website. <http://www.co2quest.eu/> (accessed: 01.07.14).
- [3] R.T.J. Porter, M. Fairweather, M. Pourkashanian, R.M. Woolley. *Int. J. Greenhouse Gas Control*, 36 (2015), pp. 161–174.
- [4] J. Wang, D. Ryan, E.J. Anthony, L. Basava-Reddi, N. Wildgust. The effect of impurities in oxyfuel flue gas on CO₂ storage capacity. *Int. J. Greenhouse Gas Control* 11, 158-162.
- [5] B. Wetenhall, J.M. Race, M.J. Downie, 2014. The effect of CO₂ purity on the development of pipeline networks for carbon capture and storage schemes. *Int. J. Greenh. Gas Control* 30, 197–211.
- [6] Cole, I.S., Corrigan, P., Sim, S., Birbilis, N., 2011. Corrosion of pipelines used for CO₂ transport in CCS: is it a real problem? *Int. J. Greenh. Gas Control* 5, 749–756.
- [7] Sim, S., Cole, I.S., Bocher, F., Corrigan, P., Gamage, R.P., Ukwattage, N., Birbilis, N., 2013. Investigating the effect of salt and acid impurities in supercritical CO₂ as relevant to the corrosion of carbon capture and storage pipelines. *Int. J. Greenh. Gas Control* 17, 534–541.
- [8] S. Brown, S. Martynov, H. Mahgerefteh, D.M. Tsangaris, G.C. Boulougouris, I.G. Economou and N.I. Diamantonis, “Impact of Equation of State on Simulating CO₂ Pipeline Decompression”, *Proc. Safety Envir. Prot.*, submitted, November 2015.
- [9] S. Brown, L.D. Peristeras, S. Martynov, R.T.J. Porter, H. Mahgerefteh, I.K. Nikolaidis, G.C. Boulougouris, D.M. Tsangaris and I.G. Economou, “Thermodynamic Interpolation for the Simulation of Two-Phase Flow of Complex Mixtures”, *J. Comput. Phys.*, submitted, March 2016.
- [10] Woolley, R. M.; Fairweather, M.; Wareing, C. J.; Proust, C.; Hebrard, J.; Jamois, D.; Narasimhamurthy, V. D.; Storvik, I. E.; Skjold, T.; Falle, S. A. E. G.; Brown, S.; Mahgerefteh, H.; Martynov, S.; Gant, S. E.; Tsangaris, D. M.; Economou, I. G.; Boulougouris, G. C.; Diamantonis, N. I., An integrated, multi-scale modelling approach for the simulation of multiphase dispersion from accidental CO₂ pipeline releases in realistic terrain. *International Journal of Greenhouse Gas Control* 2014, 27, 221-238.

- [11] Martynov, S., Brown, S., Mahgerefteh, H., Sundra, V., Chen, S., and Zhang, Y., *Modelling Three-phase Releases of Carbon Dioxide from High-pressure Pipelines. Journal of Process Safety and Environmental Protection*, 2013. 92(1): 36-46.
- [12] S. Martynov, W. Zheng, S. Brown, H. Mahgerefteh, "Numerical Simulation of CO₂ Flows in Pipes with Phase Transition Across the Triple Point". 12th International Conference on Heat Transfer, Fluid Mechanics and Thermodynamics (HEFAT2016), 11-13 July 2016, Spain.
- [13] Prausnitz, J. M.; Lichtenthaler, R. N.; de Azevedo, E. G., *Molecular Thermodynamics of Fluid-Phase Equilibria*. 3rd ed.; Prentice-Hall: New Jersey, 1999.
- [14] Seiler, M.; Groß, J.; Bungert, B.; Sadowski, G.; Arlt, W., Modeling of Solid/Fluid Phase Equilibria in Multicomponent Systems at High Pressure. *Chemical Engineering & Technology* 2001, 24 (6), 607-612.
- [15] Jäger, A.; Span, R., Equation of State for Solid Carbon Dioxide Based on the Gibbs Free Energy. *Journal of Chemical & Engineering Data* 2012, 57 (2), 590-597.
- [16] Gross, J.; Sadowski, G., Perturbed-Chain SAFT: An Equation of State Based on a Perturbation Theory for Chain Molecules. *Industrial & Engineering Chemistry Research* 2001, 40 (4), 1244-1260.
- [17] Fandiño, O.; Trusler, J. P. M.; Vega-Maza, D., Phase behavior of (CO₂ + H₂) and (CO₂ + N₂) at temperatures between (218.15 and 303.15) K at pressures up to 15 MPa. *International Journal of Greenhouse Gas Control* 2015, 36, 78-92.
- [18] Donnelly, H. G.; Katz, D. L., Phase Equilibria in the Carbon Dioxide–Methane System. *Industrial & Engineering Chemistry* 1954, 46 (3), 511-517.
- [19] Davis, J. A.; Rodewald, N.; Kurata, F., Solid-liquid-vapor phase behavior of the methane-carbon dioxide system. *AIChE Journal* 1962, 8 (4), 537-539.
- [20] Diamantonis, N. I.; Boulougouris, G. C.; Mansoor, E.; Tsangaris, D. M.; Economou, I. G., Evaluation of Cubic, SAFT, and PC-SAFT Equations of State for the Vapor–Liquid Equilibrium Modeling of CO₂ Mixtures with Other Gases. *Industrial & Engineering Chemistry Research* 2013, 52 (10), 3933-3942.
- [21] Moore, J.J., Allison, T., Lerche, A., Pacheco, J., and Delgado, H. *Development of Advanced Centrifugal Compressors and Pumps for Carbon Capture and Sequestration Applications*. in *The Fortieth Turbomachinery Symposium* 2011, Houston, Texas 107-120.
- [22] Witkowski, A. and Majkut, M., *The Impact of CO₂ Compression Systems on the Compressor Power Required for a Pulverized Coal-fired Power Plant in Post-combustion Carbon Dioxide Sequestration. The Archive of Mechanical Engineering*, 2012. 59(3).
- [23] Martynov, S. and Brown, S., *CO₂QUEST Internal Report: A Report Describing the Optimum CO₂ Compression Strategy. Deliverable 2.2, University College London, UK. 2014*.
- [24] S. Martynov, N. Daud, H. Mahgerefteh, S. Brown, R.T.J. Porter, "Impact of stream impurities on compressor power requirements for CO₂ pipeline transportation", *Int. J. Greenhouse gas Control.*, submitted, Apr 2016.

- [25] Mahgerefteh, H., Denton, G., and Rykov, Y., *A Hybrid Multiphase Flow Model*. **AIChE Journal**, 2008. 54(9): 2261-2268.
- [26] Mahgerefteh, H., Oke, A., and Atti, O., *Modelling Outflow Following Rupture in Pipeline Networks*. **Chemical Engineering Science**, 2006. 61(6): 1811-1818.
- [27] Martynov, S., Mac Dowell, N., Brown, S., and Mahgerefteh, H. (2015) Assessment of thermo-hydraulic models for pipeline transportation of dense-phase and supercritical CO₂. *Ind. Eng. Chem. Research Journal*. 2015, 54 (34), pp 8587–8599.
- [28] Brown, S., Mahgerefteh, H., Martynov, S., Sundara, V., Dowell, N.M. (2015) A multi-source flow model for CCS pipeline transportation networks. *International Journal of Greenhouse Gas Control*. 43, pp. 108-114.
- [29] Woolley, R.M., Fairweather, M., Wareing, C.J., Falle, S.A.E.G., Proust, C., Hebrard, J., and Jamois, D., *Experimental Measurement and Reynolds-Averaged Navier-Stokes Modelling of the Near-Field Structure of Multi-phase CO₂ Jet Releases*. **International Journal of Greenhouse Gas Control**, 2013. 18(1): 139-149.
- [30] Sarkar, S., *The Stabilizing Effect of Compressibility in Turbulent Shear Flow*. **Journal of Fluid Mechanics**, 1995. 282: 163-186.
- [31] Rotta, J., *Statistische Theorie nichthomogener Turbulenz. 1. Mitteilung*. **Zeitschrift für Physik A-Hadrons and Nuclei**, 1951. 129: 547-572.
- [32] Khlifi, H. and Lili, T., *A Reynolds Stress Closure for Compressible Turbulent Flow*. **Journal of Applied Fluid Mechanics**, 2011. 4(2): 99-104.
- [33] Jones, W.P. and Musonge, P., *Closure of the Reynolds Stress and Scalar Flux Equations*. **Physics of Fluids**, 1988. 31(12): 3589-3604.
- [34] Gomez, C.A. and Girimaji, S.S., *Toward Second-moment Closure Modelling of Compressible Shear Flows*. **Journal of Fluid Mechanics**, 2013. 733: 325-369.
- [35] Donaldson, C.D. and Snedeker, R.S., *A Study of Free Jet Impingement. Part 1. Mean Properties of Free and Impinging Jets*. **Journal of Fluid Mechanics**, 1971. 45(2): 281-319.
- [36] Peng, D.-Y. and Robinson, D.B., *A New Two-Constant Equation of State*. **Industrial and Engineering Chemistry Fundamentals**, 1976. 15(1): 59-64.
- [37] Span, R. and Wagner, W., *A New Equation of State for Carbon Dioxide Covering the Fluid Region from the Triple-Point Temperature to 1100 K at Pressures up to 800 MPa*. **Journal of Physical and Chemical Reference Data**, 1996. 25(6): 1509-1596.
- [38] Wareing, C.J., Woolley, R.M., Fairweather, M., and Falle, S.A.E.G., *A Composite Equation of State for the Modelling of Sonic Carbon Dioxide Jets*. **American Institute of Chemical Engineers Journal**, 2013. 59(10): 3928-3942.
- [39] Jager, A. and Span, R., *Equation of State for Solid Carbon Dioxide Based on the Gibbs Free Energy*. **Journal of Chemical and Engineering Data**, 2012. 57: 590-597.
- [40] Yokozeki, A., *Solid–Liquid–Vapor Phases of Water and Water–Carbon Dioxide Mixtures Using a Simple Analytical Equation of State*. **Fluid Phase Equilibria**, 2004. 222-223: 55-66.

- [41] CO2PipeHaz. *Quantitative Failure Consequence Hazard Assessment for Next Generation CO₂ Pipelines: The Missing Link*, 2009. Accessed 11/11/14; [CO2PipeHaz Project Website]. Available from: <http://www.co2pipehaz.eu/>.
- [42] Jamois, D., Proust, C., and Hebrard, J., *Hardware and Instrumentation to Investigate Massive Spills of Dense Phase CO₂*. **Chemical Engineering Transactions**, 2014. 36: 601-606.
- [43] R. Talemi, S. Brown, S. Martynov, H. Mahgerefteh, "A hybrid fluid-structure interaction modelling of dynamic brittle fracture in pipeline steel transporting CO₂ streams", *Int. J. Greenhouse gas Control.*, submitted, Apr 2016.
- [44] Talemi, S. Brown, S. Martynov, H. Mahgerefteh, "Assessment of brittle fractures in CO₂ transportation pipelines: A hybrid fluid-structure interaction model", 21st European Conference on Fracture, ECF21, 20-24 June 2016, Catania, Italy. Structural Integrity Procedia, Submitted, April 2016.
- [45] Niemi, A., Bensabat, J., Shtivelman, V., Edlmann, K., Gouze, P., Linda Luquot, L., Hingerl, F., Benson, S. M., Pezard P. A., Rasmusson, K., Liang, T., Fagerlund, F., Gendler, M., Goldberg, I., Tatomir, A., Lange, T., Sauter, M., and Freifeld, B., *Heletz experimental site overview, characterization and data analysis for CO₂ injection and geological storage*. **International Journal of Greenhouse Gas Control**, 2016, in press.
- [46] Rebscher, D., Wolf, J. L., Jung, B., Bensabat, and A. Niemi, Numerical simulations of the chemical impact of impurities on geological CO₂ storage – Comparison between TOUGHREACT V2.0 and TOUGHREACT V3.0-OMP, 2015, **LBNL-190559**, Proceedings, TOUGH Symposium 2015, Lawrence, Berkeley National Laboratory, Berkeley, California, September 28-30, 2015, 493-500, http://esd1.lbl.gov/files/research/projects/tough/events/symposia/toughsymposium15/Proceedings_TOUGHSymposium2015.pdf
- [47] Xu, T., Sonnenthal, E. Spycher, N., and Zheng, L., *TOUGHREACT V3.0-OMP Reference Manual: A Parallel Simulation Program for Non-Isothermal Multiphase Geochemical Reactive Transport*, **LBNL-DRAFT**, Lawrence Berkeley National Laboratory, Berkeley, California, 2014, http://esd1.lbl.gov/files/research/projects/tough/documentation/TOUGHREACT_V3-OMP_RefManual.pdf
- [48] Pan, L., Spycher, N., Doughty, C., and K. Pruess, *ECO2N V2.0: A TOUGH2 Fluid Property Module for Mixtures of Water, NaCl and CO₂*, **LBNL-6930E**, Lawrence Berkeley National Laboratory, Berkeley, California, 2015, http://esd1.lbl.gov/files/research/projects/tough/documentation/TOUGH2-ECO2N_V2.0_Users_Guide.pdf.
- [49] Grossmann, I.E. and Sargent, R.W.H., *Optimum design of multipurpose chemical plants*. **Industrial and Engineering Chemistry Process Design and Development**, 1979. 18(2): 343-348.
- [50] Arce, A., Mac Dowell, N., Shah, N., and Vega, L.F., *Flexible operation of solvent regeneration systems for CO₂ capture processes using advanced control techniques: Towards operational cost minimisation*. **International Journal of Greenhouse Gas Control**, 2012. 11: 236-250.

- [51] Mac Dowell, N. *Optimisation of post-combustion CCS for flexible operation*. in *The 14th Annual APGTF Workshop - 'The Role of Fossil Fuel Power Plant in Providing Flexible Generation'* 2014, London.
- [52] Mac Dowell, N., Galindo, A., Jackson, G., and Adjiman, C.S., *Integrated solvent and process design for the reactive separation of CO₂ from flue gas*. **Computer Aided Chemical Engineering**, 2010. 28: 1231-1236.
- [53] Mac Dowell, N., Pereira, F.E., Llovel, F., Blas, F.J., Adjiman, C.S., Jackson, G., and Galindo, A., *Transferable SAFT-VR models for the calculation of the fluid phase equilibria in reactive mixtures of carbon dioxide, water, and n-alkylamines in the context of carbon capture*. **Journal of Physical Chemistry B**, 2011. 115(25): 8155-8168.
- [54] Mac Dowell, N., Samsatli, N.J., and Shah, N., *Dynamic modelling and analysis of an amine-based post-combustion CO₂ capture absorption column*. **International Journal of Greenhouse Gas Control**, 2013. 12: 247-258.
- [55] Mac Dowell, N. and Shah, N., *Dynamic modelling and analysis of a coal-fired power plant integrated with a novel split-flow configuration post-combustion CO₂ capture process*. **International Journal of Greenhouse Gas Control**, 2014. 27: 103-119.
- [56] Mac Dowell, N. and Shah, N., *The multi-period operation of an amine-based CO₂ capture process integrated with a supercritical coal-fired power station*. **Computers and Chemical Engineering**, 74, (2015) 169–183.
- [57] Rodriguez, J., Mac Dowell, N., Llovel, F., Adjiman, C.S., Jackson, G., and Galindo, A., *Modelling the fluid phase behaviour of aqueous mixtures of multifunctional alkanolamines and carbon dioxide using transferable parameters with the SAFT-VR approach*. **Molecular Physics**, 2012. 110(11-12): 1325-1348.
- [58] Mac Dowell, N. and Shah, N., *Identification of the cost-optimal degree of CO₂ capture: An optimisation study using dynamic process models*. **International Journal of Greenhouse Gas Control**, 2013. 13: 44-58.
- [59] CO₂QUEST Newsletter Autumn 2014, *Impact of the Quality of CO₂ stream on Storage and Transport*, http://www.co2quest.eu/main_download/newsletters/CO2QUEST_newsletter_Autumn_2014.pdf